Commun Nonlinear Sci Numer Simulat 151 (2025) 109055

Contents lists available at ScienceDirect

Communications in Nonlinear Science and Numerical Simulation

journal homepage: www.elsevier.com/locate/cnsns

Research paper

Application of a reflected forward backward splitting method with momentum to a fractional-order lung cancer model

Chinedu Izuchukwu [a,b,*], David Amilo [c,d], Khadijeh Sadri [c,d], Hao-Ren Yao [e], Jen-Chih Yao [f]

[a] School of Mathematics, University of the Witwatersrand, Private Bag 3, Johannesburg, 2050, South Africa
[b] DSI-NRF Centre of Excellence in Mathematical and Statistical Sciences (CoE-MaSS), South Africa
[c] Mathematics Research Center, Near East University TRNC, Mersin 10, Nicosia 99138, Turkey
[d] Department of Mathematics, Near East University TRNC, Mersin 10, Nicosia 99138, Turkey
[e] The Language Technologies Institute, Carnegie Mellon University, Pittsburgh, PA, USA
[f] Center for General Education, China Medical University, Taichung 40402, Taiwan

ARTICLE INFO

MSC:
47H09
47H10
49J20
49J40

Keywords:
Reflected-forward–backward method
Momentum term
Monotone inclusion
Monotone operators
Lung cancer
Fractional-order model

ABSTRACT

We introduce in this paper, a reflected-forward–backward splitting method that integrates momentum terms to improve the resolution of monotone inclusion problems involving a maximal monotone operator and a monotone Lipschitz continuous operator in a Hilbert space. Momentum terms are integrated to leverage historical information about iterates, thus improving convergence speed. The method that we propose requires one forward computation of the single-valued operator with one backward computation of the set-valued operator per iteration, a key advantage over many existing inertial splitting methods. The practical potential of this method is demonstrated through its application to a fractional-order lung cancer model, where the proposed method showcases its ability to handle complex biological dynamics with improved computational accuracy and reliability. This study makes a significant contribution by demonstrating the method's versatility in addressing real-world problems involving biological models.

1. Introduction

Monotone inclusion problems, characterized by finding zeros of the sum of a set-valued monotone operator $\mathcal{J} : \mathcal{V} \to 2^{\mathcal{V}}$ and a single-valued monotone operator $\mathcal{K} : \mathcal{V} \to \mathcal{V}$, within the context of a real Hilbert space $\mathcal{V}$, have become increasingly prominent in the fields of optimization, variational analysis, and applied mathematics. This problem is modeled as

$$\text{find } e^* \in \mathcal{V} \text{ such that } 0 \in (\mathcal{J} + \mathcal{K})e^*. \tag{1.1}$$

If $\mathcal{J} = \partial h$ and $\mathcal{K} = \nabla T$, the subdifferential of a proper and convex function that is lower semicontinuous $h : \mathcal{V} \to (-\infty, +\infty]$ and the gradient of a differentiable function that is convex $T : \mathcal{V} \to \mathbb{R}$, respectively, then the monotone inclusion problem (1.1) reduces to the following composite convex optimization problem:

$$\min_{e \in \mathcal{V}} \{h(e) + T(e)\}. \tag{1.2}$$

* Corresponding author at: School of Mathematics, University of the Witwatersrand, Private Bag 3, Johannesburg, 2050, South Africa.
E-mail addresses: chinedu.izuchukwu@wits.ac.za (C. Izuchukwu), amilodavid.ikechukwu@neu.edu.tr (D. Amilo), khadijeh.sadrikhatouni@neu.edu.tr (K. Sadri), haoreny@cs.cmu.edu (H.-R. Yao), yaojc@mail.cmu.edu.tw (J.-C. Yao).

https://doi.org/10.1016/j.cnsns.2025.109055
Received 5 March 2025; Received in revised form 30 May 2025; Accepted 3 June 2025
Available online 17 June 2025

The solutions to (1.2) satisfy the first order optimality condition:

$$\text{find } e^* \in \mathcal{V} \text{ such that } 0 \in (\partial h + \nabla T)e^*.$$

To provide further motivating examples for problem (1.1), let us look at the saddle point problem:

$$\min_{e\in\mathcal{V}} \max_{f\in\mathcal{V}} h_1(e) + F(e,\ f) - h_2(f), \tag{1.3}$$

where $h_1, h_2 : \mathcal{V} \to (-\infty, +\infty]$ are proper and convex functions that are also lower semicontinuous and $F : \mathcal{V}\times\mathcal{V} \to \mathbb{R}$ is a smooth function that is also convex-concave. We can recast problem (1.3) as:

$$\text{find } \begin{pmatrix} e^* \\ f^* \end{pmatrix} \in \mathcal{V}\times\mathcal{V} \text{ such that } \begin{pmatrix} 0 \\ 0 \end{pmatrix} \in \begin{pmatrix} \partial h_1(e^*) \\ \partial h_2(f^*) \end{pmatrix} + \begin{pmatrix} \nabla_{e^*} F(e^*,\ f^*) \\ -\nabla_{f^*} F(e^*,\ f^*) \end{pmatrix}. \tag{1.4}$$

The point $(e^*,\ f^*)'$ characterizes the solution to problem (1.3). We can also recast problem (1.4) as the following generalized mixed variational inequality problem [1,2]:

$$\text{find } c^* = (e^*,\ f^*)' \in \mathcal{V}\times\mathcal{V} \text{ such that } \langle \mathcal{K}c^*, c - c^*\rangle + h_1(e) - h_1(e^*) + h_2(f) - h_2(f^*) \geq 0 \ \ \forall c = \begin{pmatrix} e \\ f \end{pmatrix} \in \mathcal{V}\times\mathcal{V},$$

where $\mathcal{K}(e^*,\ f^*)' = (\nabla_{e^*} F(e^*,\ f^*),\ -\nabla_{f^*} F(e^*,\ f^*))'$.

Thus, problem (1.1) can be seen as an important aspect of mathematical optimization. It also arises naturally in diverse disciplines, including signal processing, control systems, biological/medical modeling and machine learning. A major challenge in solving such problems is the computational complexity associated with large-scale systems, which often demand efficient and scalable methods. To address this challenge, researchers have turned to splitting methods, which divide the problem into smaller, manageable sub-problems involving individual operators. This paper emphasizes the use of these splitting methods in biological modeling, particularly, lung cancer modeling. Lung cancer remains a major contributor to cancer-related deaths globally, highlighting the need for advanced models to analyze its progression and develop effective therapeutic strategies [3]. Traditional integer-order models often fail to capture the complex, nonlinear behaviors characteristic of biological systems, leading to a need for more accurate and flexible approaches. In this context, fractional-order models have emerged as a powerful tool, offering enhanced accuracy by incorporating memory effects which enable them to incorporate past states and events that are important in understanding disease progression [4,5]. This leads to high accuracy and sophisticated representation of biological processes. Furthermore, fractional-order models offer more flexibility when explaining how different parts of the biological system interact leading to a better understanding of mechanisms underlying tumour growth, metastasis, and immune response, thus providing a more comprehensive and reliable picture of lung cancer trends [6,7].

Among the prominent splitting methods, the classical forward–backward splitting method offers simple frameworks in handling monotone inclusion problems [8,9]:

$$m_{i+1} = (I_{\mathcal{V}} + \sigma\mathcal{J})^{-1}(m_i - \sigma\mathcal{K}m_i),\ i \geq 1, \tag{1.5}$$

where $I_{\mathcal{V}}$ refers to the identity operator defined on $\mathcal{V}$, while σ refers to a positive parameter. It operates by iteratively combining a forward step for the single-valued operator $\mathcal{K}$ with a backward step for the set-valued operator $\mathcal{J}$, ensuring convergence under the cocoercive assumption of the $\mathcal{K}$ which is strict.

In [10], the strict cocoercivity requirement for Method (1.5) was eliminated by introducing the forward–backward-forward splitting method, commonly recognized as Tseng's algorithm. This approach is formulated as:

$$\begin{cases} n_i = (I_{\mathcal{V}} + \sigma\mathcal{J})^{-1}(m_i - \sigma\mathcal{K}m_i), \\ m_{i+1} = n_i - \sigma\mathcal{K}n_i + \sigma\mathcal{K}m_i,\ i \geq 1. \end{cases} \tag{1.6}$$

Researchers have extensively examined variations of this method, including its inexact [11], variable metric [12], and stochastic [13] forms. A key advantage is its convergence to a solution of (1.1) under relaxed conditions: $\mathcal{K}$ must be $\mathcal{L}$-Lipschitz continuous and also monotone, σ must be in the interval $(0, \mathcal{L}^{-1})$, $\mathcal{J}$ needs to be maximal monotone, and $(\mathcal{J}+\mathcal{K})^{-1}(0) \neq \emptyset$, which is the solution set, must be nonempty. However, its significant drawback is the need for two forward evaluations of $\mathcal{K}$ per iteration, which can reduce efficiency, especially in computationally demanding large-scale optimization or control problems [14].

To mitigate this issue, [15] proposed an alternative method: the forward-reflected-backward splitting method. This variant is expressed as:

$$m_{i+1} = (I_{\mathcal{V}} + \sigma\mathcal{J})^{-1}(m_i - 2\sigma\mathcal{K}m_i + \sigma\mathcal{K}m_{i-1}),\ i \geq 1, \tag{1.7}$$

with the step size parameter σ restrcited to $(0, \frac{1}{2}\mathcal{L}^{-1})$. Method (1.7) involves a single forward computation of the operator $\mathcal{K}$, enhancing computational efficiency while maintaining applicability to monotone and Lipschitz continuous operators. An extension for reflexive Banach spaces is discussed in [16].

When $\mathcal{K}$ is linear, the structure of Method (1.7) aligns with the reflected-forward–backward splitting method [17], and is defined as:

$$\begin{cases} n_i = 2m_i - m_{i-1} \\ m_{i+1} = (I_{\mathcal{V}} + \sigma\mathcal{J})^{-1}(m_i - \sigma\mathcal{K}n_i),\ i \geq 1. \end{cases} \tag{1.8}$$

The weak convergence properties of Method (1.8) have been analyzed with various conditions in [17], for cases where $\mathcal{J}$ is maximal monotone (in [18]), under the assumption that $\mathcal{J}$ represents the normal cone of a certain subset of $\mathcal{V}$. Additionally, the line-search adaptation of method (1.8) was explored in [19] in which $\mathcal{J}$ represents the subdifferential of a proper and convex function that is also lower semicontinuous.

In recent years, fast converging optimization problem-solving methods have garnered significant interest. They are inspired by second-order differential equations, and have proven effective in enhancing the convergence speed of optimization problem-solving methods (see [20–25]). This desire for faster convergence has led to the development of momentum techniques. The momentum term amplifies the contribution of past iterates, effectively acting as a memory mechanism that stabilizes the iterative process and accelerates convergence. Momentum terms offer several advantages over traditional optimization methods, making them particularly useful in a broad spectrum of applications, especially in high-dimensional and large-scale optimization problems [21,22]. One of the primary benefits of methods that integrate momentum terms is their ability to expedite the convergence of iterative procedures. Such methods can significantly reduce the iteration count needed to reach an optimal result compared to traditional methods. This is particularly valuable in scenarios where computational resources or time are limited. Furthermore, methods with momentum terms are well-suited for optimization tasks that frequently occur in machine learning [26], data science [27], and signal processing. Their ability to accelerate convergence means that they can handle larger datasets and higher-dimensional spaces more efficiently. This scalability is crucial for modern applications that involve massive amounts of data [27], like the complex biological dynamics that we considered in Section 4. Moreover, such methods can reduce the overall computational cost of solving optimization problems by accelerating the convergence rate. This is particularly beneficial in applications where each iteration is computationally expensive, such as in large-scale machine learning models or complex simulations. For notable results on fast convergent methods for addressing problem (1.1), see [24,25] and the sources cited therein.

Building on the discussion above, we investigate the role of the momentum term in the reflected-forward–backward splitting method. Unlike traditional splitting methods, our proposed method incorporates momentum directly into the reflected and forward–backward steps, resulting in improved numerical performance. This makes the method particularly suited for large-scale applications where computational efficiency and convergence speed are critical. Applications to a fractional-order lung cancer model further highlight the practical benefits of the momentum-enhanced approach.

2. Preliminaries

For a sequence m_i in $\mathcal{V}$ and a point e in $\mathcal{V}$, strong convergence of m_i to e is written as $m_i \to e$, while weak convergence is denoted by $m_i \rightharpoonup e$.

The operator $\mathcal{K} : \mathcal{V} \to \mathcal{V}$ is referred to as $\mathcal{L}$-cocoercive if there is a constant $\mathcal{L} > 0$ such that

$$\langle \mathcal{K}e - \mathcal{K}c, e - c\rangle \geq \mathcal{L}\|\mathcal{K}e - \mathcal{K}c\|^2 \ \forall e, c \in \mathcal{V},$$

and monotone if

$$\langle \mathcal{K}e - \mathcal{K}c, e - c\rangle \geq 0 \ \ \forall e, c \in \mathcal{V}.$$

The operator $\mathcal{K}$ is referred to as an $\mathcal{L}$-Lipschitz continuous operator if there is $\mathcal{L} > 0$ such that

$$\|\mathcal{K}e - \mathcal{K}c\| \leq \mathcal{L}\|e - c\| \ \forall e, c \in \mathcal{V}.$$

Let $\mathcal{J}$ be a set-valued operator $\mathcal{J} : \mathcal{V} \to 2^{\mathcal{V}}$, $\mathcal{J}$ is referred to as a monotone operator if

$$\langle f - g, e - c\rangle \geq 0 \ \ \forall e, c \in \mathcal{V}, \ f \in \mathcal{J}e, \ g \in \mathcal{J}c,$$

and strongly monotone if there is $\epsilon > 0$ such that

$$\langle f - g, e - c\rangle \geq \epsilon\|e - c\|^2 \ \ \forall e, c \in \mathcal{V}, \ g \in \mathcal{J}e, \ g \in \mathcal{J}c.$$

$\mathcal{J}$ is termed a maximal monotone operator if the graph of $\mathcal{J}$, $\mathcal{G}(\mathcal{J})$ given as

$$\mathcal{G}(\mathcal{J}) := \{(e, f) \in \mathcal{V} \times \mathcal{V} : f \in \mathcal{J}e\},$$

is not a proper subset of the graph of any other monotone operator. Specifically, $\mathcal{J}$ is termed maximal monotone if, for $(e, f) \in \mathcal{V}\times\mathcal{V}$, we have that $\langle f - g, e - c\rangle \geq 0$ for all $(c, g) \in \mathcal{G}(\mathcal{J})$ implies $f \in \mathcal{J}e$. Associated with a set-valued operator $\mathcal{J}$ is the resolvent, which is defined as the mapping $J_\sigma^{\mathcal{J}} : \mathcal{V} \to 2^{\mathcal{V}}$ given by

$$J_\sigma^{\mathcal{J}}(e) := (I_{\mathcal{V}} + \sigma\mathcal{J})^{-1}(e), \quad e \in \mathcal{V}, \ \sigma > 0.$$

When the monotone operator $\mathcal{J}$ is maximal and $\mathcal{K}$ is single-valued, both $J_\sigma^{\mathcal{J}}$ and $J_\sigma^{\mathcal{J}}(I_{\mathcal{V}} - \sigma\mathcal{K})$ are guaranteed to be single-valued and are defined everwhere in the entire space $\mathcal{V}$.

The following identities holds:

$$2\langle q, j\rangle = \|q\|^2 + \|j\|^2 - \|q - j\|^2 = \|q + j\|^2 - \|q\|^2 - \|j\|^2, \forall q, j \in \mathcal{V} \tag{2.1}$$

and

$$\|\bar{\xi}\ q + (1 - \bar{\xi})j\|^2 = \bar{\xi}\|q\|^2 + (1 - \bar{\xi})\|j\|^2 - \bar{\xi}(1 - \bar{\xi})\|q - j\|^2, \ \forall q, j \in \mathcal{V}, \ \bar{\xi} \in \mathbb{R}. \tag{2.2}$$

Definition 2.1. Consider $\gamma \in \mathbb{R}$ satisfying $i-1 < \gamma \leq i$, where $i \in \mathbb{N}$, and let h be absolutely continuous over $[0,\infty)$. The Caputo fractional derivative of order γ is given by:

$$ {}_0^c D_t^\gamma h(t) = \frac{1}{\Gamma(i-\gamma)} \int_0^t (t-s)^{i-\gamma-1} h^{(i)}(s)\, ds, \quad t \in [0, T_h],\ \gamma \in (0,1], $$

where $h^{(i)}$ means h is a function that is differentiable i times, and Γ represents the Gamma function, defined by

$$ \Gamma(e) = \int_0^\infty \exp(z)\, z^{e-1}\, dz, \quad Re(z) > 0. $$

Definition 2.2. The fractional integral of h in the sense of Riemann–Liouville, for an order $\gamma > 0$, is given by

$$ {}_0^{RL} I_t^\gamma h(t) = \frac{1}{\Gamma(\gamma)} \int_0^t (t-s)^{\gamma-1} h(s)\, ds, \quad t \in [0, T_f]. $$

For any function h that is absolutely integrable, the integral is valid almost everywhere.

Lemma 2.3 ([28]). *Consider a closed, nonempty subset $\mathcal{Q}$ of $\mathcal{V}$ and a bounded sequence $\{m_i\}$ in $\mathcal{V}$. If all weak sequential cluster points of $\{m_i\}$ lie within $\mathcal{Q}$, then the sequence $\{m_i\}$ weakly converges to some point in $\mathcal{Q}$.*

3. Description of the proposed method and its weak convergence analysis

This section introduces the proposed method and provides a proof of its weak convergence theorem, starting with the conditions outlined below.

Assumption 3.1.

(a) $\mathcal{J}$ is maximal monotone,
(b) $\mathcal{K}$ is monotone and Lipschitz continuous with Lipschitz constant $\mathcal{L} > 0$,
(c) $(\mathcal{J}+\mathcal{K})^{-1}(0)$ is nonempty.

Algorithm 3.2. Inertial Reflected-Forward-Backward Splitting Method with Momentum.

Let $\sigma > 0$ and $\varrho \geq 0$. For arbitrary $m_0, m_1, q_1 \in \mathcal{V}$, let the sequence $\{m_i\}$ be generated by

$$ \begin{cases} w_i = \frac{1}{1+\varrho} m_i + \frac{\varrho}{1+\varrho} q_i \\ n_i = 2m_i - m_{i-1} \\ m_{i+1} = J_\sigma^{\mathcal{J}}(w_i - \sigma \mathcal{K} n_i) \\ q_{i+1} = \frac{1}{1+\varrho} m_{i+1} + \frac{\varrho}{1+\varrho} q_i, \ i \geq 1. \end{cases} $$

Description of Algorithm 3.2:

Initialization:

- Start with arbitrary initial values m_0, m_1, and q_1 in the Hilbert space $\mathcal{V}$.
- Parameters $\sigma > 0$ (step size) and $\varrho \geq 0$ (momentum parameter).

Step 1: Weighted Combination for Momentum:

$$ w_i = \frac{1}{1+\varrho} m_i + \frac{\varrho}{1+\varrho} q_i. $$

- *Description:* Combines the current iterate m_i and the auxiliary iterate q_i with weights determined by the momentum parameter ϱ.
- *Momentum Role:* The term $\frac{\varrho}{1+\varrho} q_i$ introduces a history-dependent component, contributing to an inertial effect.

Step 2: Reflection Step:

$$ n_i = 2m_i - m_{i-1}. $$

- *Description:* This step extrapolates n_i by reflecting m_{i-1} about m_i. It is called the reflected step because it uses the symmetry inherent in the operation:

$$ n_i - m_i = m_i - m_{i-1}. $$

The reflected step allows the algorithm to "look ahead" by leveraging the trend between the current iterate (m_i) and the previous one (m_{i-1}). It also contributes to the algorithm's inertial behavior, as it incorporates differences between successive iterates ($m_i - m_{i-1}$). This is particularly valuable in accelerating convergence for optimization or monotone inclusion problems. Thus, it is a hallmark of the reflected variants of splitting algorithms.

- *Role:* The reflected step plays a dual role:
  - It is the reflected component of the reflected-forward–backward splitting framework.
  - It also serves as an inertial component, indirectly introducing a momentum-like effect by amplifying the contribution of past iterates.

Step 3: Reflective Forward-Backward Update:

$$m_{i+1} = J_\sigma^{\mathcal{J}}(w_i - \sigma \mathcal{K} n_i).$$

- *Description:* - $J_\sigma^{\mathcal{J}} = (I + \sigma\mathcal{J})^{-1}$ is the resolvent operator for $\mathcal{J}$, which also represents the backward evaluation of $\mathcal{J}$. - The update uses the weighted point w_i and the forward evaluation of the monotone operator $\mathcal{K}$ at n_i.
- *Momentum Role:* The extrapolated n_i indirectly incorporates inertial information into the resolvent computation.

Step 4: Auxiliary Sequence Update:

$$q_{i+1} = \frac{1}{1+\varrho} m_{i+1} + \frac{\varrho}{1+\varrho} q_i.$$

- *Description:* Updates the auxiliary variable q_{i+1} using the new iterate m_{i+1} and the previous auxiliary variable q_i.
- *Momentum Role:* Again, the term $\frac{\varrho}{1+\varrho} q_i$ ensures that the memory of past iterates influences the update.

Lemma 3.3. *Let Algorithm 3.2 generate $\{m_i\}$ and let the conditions outlined in Assumption 3.1 be met. For all $e \in (\mathcal{J}+\mathcal{K})^{-1}(0)$ and for $\epsilon > 1$, define*

$$\begin{aligned} a_i \;:=\; & \frac{1}{1+\varrho}\|m_i - e\|^2 + \varrho\|q_i - e\|^2 + \frac{\varrho^2}{\epsilon(1+\varrho)^2}\|m_i - q_{i-1}\|^2 + \|m_i - m_{i-1}\|^2 + \sigma\mathcal{L}\|m_i - n_{i-1}\|^2 \\ & + \|p_i + \sigma\mathcal{K}e\|^2 - \|p_i + m_i - m_{i-1} + \sigma\mathcal{K}e\|^2, \end{aligned} \tag{3.1}$$

where

$$p_i := w_{i-1} - \sigma\mathcal{K}n_{i-1} - m_i. \tag{3.2}$$

Then

$$a_{i+1} \le a_i - \left(\frac{\epsilon-1}{\epsilon}\right)\frac{\varrho^2}{(1+\varrho)^2}\|m_{i+1} - q_i\|^2 - \left(1 - \frac{\epsilon\varrho^2}{(1+\varrho)^2} - \frac{\varrho}{1+\varrho} - \sigma\mathcal{L}(1+\sqrt{2})\right)\left[\|m_{i+1} - n_i\|^2 + \|n_i - m_i\|^2\right].$$

Proof. Let $e \in (\mathcal{J}+\mathcal{K})^{-1}(0)$. From $m_i = J_\sigma^{\mathcal{J}}(w_{i-1} - \sigma\mathcal{K}n_{i-1})$, the definition of $J_\sigma^{\mathcal{J}}$ and (3.2), we get $p_i \in \sigma\mathcal{J}m_i$.
Similarly, $p_{i+1} \in \sigma\mathcal{J}m_{i+1}$. Also,

$$2\langle m_i - w_{i-1} + p_i + \sigma\mathcal{K}n_{i-1}, m_{i+1} - n_i\rangle = 0 \tag{3.3}$$

and

$$2\langle m_{i+1} - w_i + p_{i+1} + \sigma\mathcal{K}n_i, e - m_{i+1}\rangle = 0. \tag{3.4}$$

Adding (3.3) and (3.4), and noting that $n_{i-1} = 2m_{i-1} - m_{i-2}$ and $w_{i-1} = \frac{1}{1+\varrho}m_{i-1} + \frac{\varrho}{1+\varrho}q_{i-1}$, we obtain for $\epsilon > 1$ that

$$\begin{aligned} 0 \;=\; & 2\langle m_i - w_{i-1}, m_{i+1} - n_i\rangle + 2\langle p_i + \sigma\mathcal{K}n_{i-1}, m_{i+1} - n_i\rangle \\ & + 2\langle m_{i+1} - w_i, e - m_{i+1}\rangle + 2\langle p_{i+1} + \sigma\mathcal{K}n_i, e - m_{i+1}\rangle \\ =\; & 2\langle m_i - w_{i-1}, m_{i+1} - n_i\rangle + 2\langle p_i + \sigma\mathcal{K}n_i, m_{i+1} - n_i\rangle + 2\sigma\langle\mathcal{K}n_{i-1} - \mathcal{K}n_i, m_{i+1} - n_i\rangle \\ & + 2\langle m_{i+1} - w_i, e - m_{i+1}\rangle + 2\langle p_{i+1} + \sigma\mathcal{K}n_i, e - m_{i+1}\rangle \\ =\; & 2\langle m_i - m_{i-1} + \frac{\varrho}{1+\varrho}m_{i-1} - \frac{\varrho}{1+\varrho}q_{i-1}, m_{i+1} - n_i\rangle + 2\langle p_i + \sigma\mathcal{K}n_i, m_{i+1} - n_i\rangle \\ & + 2\sigma\langle\mathcal{K}n_{i-1} - \mathcal{K}n_i, m_{i+1} - n_i\rangle + 2\langle m_{i+1} - w_i, e - m_{i+1}\rangle + 2\langle p_{i+1} + \sigma\mathcal{K}n_i, e - m_{i+1}\rangle \\ =\; & 2\langle m_i - m_{i-1} + \frac{\varrho}{1+\varrho}\left[(m_i - q_{i-1}) - (m_i - m_{i-1})\right], m_{i+1} - n_i\rangle + 2\langle p_i + \sigma\mathcal{K}n_i, m_{i+1} - n_i\rangle \\ & + 2\sigma\langle\mathcal{K}n_{i-1} - \mathcal{K}n_i, m_{i+1} - n_i\rangle + 2\langle m_{i+1} - w_i, e - m_{i+1}\rangle + 2\langle p_{i+1} + \sigma\mathcal{K}n_i, e - m_{i+1}\rangle \\ =\; & 2\langle\left(1 - \frac{\varrho}{1+\varrho}\right)(m_i - m_{i-1}) + \frac{\varrho}{1+\varrho}(m_i - q_{i-1}), m_{i+1} - n_i\rangle + 2\langle p_i + \sigma\mathcal{K}n_i, m_{i+1} - n_i\rangle \end{aligned}$$

$$
\begin{aligned}
&+2\sigma\langle \mathcal{K}n_{i-1}-\mathcal{K}n_i, m_{i+1}-n_i\rangle + 2\langle m_{i+1}-w_i, e-m_{i+1}\rangle + 2\langle p_{i+1}+\sigma\mathcal{K}n_i, e-m_{i+1}\rangle\\
&= 2\langle\left(1-\frac{\varrho}{1+\varrho}\right)(n_i-m_i)+\frac{\varrho}{1+\varrho}(m_i-q_{i-1}), m_{i+1}-n_i\rangle + 2\langle p_i+\sigma\mathcal{K}n_i, m_{i+1}-n_i\rangle\\
&\quad +2\sigma\langle \mathcal{K}n_{i-1}-\mathcal{K}n_i, m_{i+1}-n_i\rangle + 2\langle m_{i+1}-w_i, e-m_{i+1}\rangle + 2\langle p_{i+1}+\sigma\mathcal{K}n_i, e-m_{i+1}\rangle\\
&\leq \frac{1}{1+\varrho}\|m_{i+1}-m_i\|^2 + \left(\frac{\epsilon\varrho^2}{(1+\varrho)^2}-\frac{1}{1+\varrho}\right)\|m_{i+1}-n_i\|^2 - \frac{1}{1+\varrho}\|m_i-n_i\|^2\\
&\quad +\frac{\varrho^2}{\epsilon(1+\varrho)^2}\|m_i-q_{i-1}\|^2 + 2\langle p_i, m_{i+1}-n_i\rangle + 2\sigma\langle \mathcal{K}n_i, e-n_i\rangle + 2\langle p_{i+1}, e-m_{i+1}\rangle\\
&\quad +2\sigma\langle \mathcal{K}n_{i-1}-\mathcal{K}n_i, m_{i+1}-n_i\rangle + \|w_i-e\|^2 - \|m_{i+1}-e\|^2 - \|m_{i+1}-w_i\|^2. \qquad (3.5)
\end{aligned}
$$

Using (2.1), we see that

$$
\begin{aligned}
\|m_{i+1}-w_i\|^2 &= \|(m_{i+1}-m_i)-\frac{\varrho}{1+\varrho}(q_i-m_i)\|^2\\
&= \|m_{i+1}-m_i\|^2 + \left(\frac{\varrho}{1+\varrho}\right)^2\|q_i-m_i\|^2 - \frac{2\varrho}{1+\varrho}\langle m_{i+1}-m_i, q_i-m_i\rangle\\
&\geq \|m_{i+1}-m_i\|^2 + \left(\frac{\varrho}{1+\varrho}\right)^2\|q_i-m_i\|^2 - \frac{\varrho}{1+\varrho}\left[\|m_{i+1}-m_i\|^2+\|q_i-m_i\|^2\right]\\
&= \frac{1}{1+\varrho}\|m_{i+1}-m_i\|^2 - \frac{\varrho}{(1+\varrho)^2}\|q_i-m_i\|^2. \qquad (3.6)
\end{aligned}
$$

Also, by (2.2), we get

$$
\begin{aligned}
\|w_i-e\|^2 &= \|\frac{1}{1+\varrho}(m_i-e)+\frac{\varrho}{1+\varrho}(q_i-e)\|^2\\
&= \frac{1}{1+\varrho}\|m_i-e\|^2 + \frac{\varrho}{1+\varrho}\|q_i-e\|^2 - \frac{\varrho}{(1+\varrho)^2}\|m_i-q_i\|^2. \qquad (3.7)
\end{aligned}
$$

Next, the Lipschitzian of $\mathcal{K}$ implies

$$
\begin{aligned}
2\sigma\langle \mathcal{K}n_{i-1}-\mathcal{K}n_i, m_{i+1}-n_i\rangle &\leq 2\sigma\mathcal{L}\|n_i-n_{i-1}\|\|m_{i+1}-n_i\|\\
&\leq \sigma\mathcal{L}\left(\frac{1}{\sqrt{2}}\|n_i-n_{i-1}\|^2+\sqrt{2}\|m_{i+1}-n_i\|^2\right)\\
&\leq \sigma\mathcal{L}\frac{1}{\sqrt{2}}((2+\sqrt{2})\|n_i-m_i\|^2+\sqrt{2}\|m_i-n_{i-1}\|^2)+\sqrt{2}\sigma\mathcal{L}\|m_{i+1}-n_i\|^2\\
&= \sigma\mathcal{L}(1+\sqrt{2})\|n_i-m_i\|^2+\sigma\mathcal{L}\|m_i-n_{i-1}\|^2+\sqrt{2}\sigma\mathcal{L}\|m_{i+1}-n_i\|^2. \qquad (3.8)
\end{aligned}
$$

Now, since $\mathcal{K}$ is monotone, we have

$$\sigma\langle \mathcal{K}n_i, e-n_i\rangle \leq \sigma\langle \mathcal{K}e, e-n_i\rangle. \qquad (3.9)$$

Also, since $p_{i+1}\in\sigma\mathcal{J}m_{i+1}$, $-\sigma\mathcal{K}e\in\sigma\mathcal{J}e$ and $\mathcal{J}$ is monotone, we have that $0\leq\langle -\sigma\mathcal{K}e-p_{i+1}, e-m_{i+1}\rangle$.
Hence,

$$
\begin{aligned}
\langle p_{i+1}, e-m_{i+1}\rangle &\leq \langle p_{i+1}, e-m_{i+1}\rangle + \langle -\sigma\mathcal{K}e-p_{i+1}, e-m_{i+1}\rangle\\
&= \sigma\langle \mathcal{K}e, m_{i+1}-e\rangle. \qquad (3.10)
\end{aligned}
$$

Again, since $p_i\in\sigma\mathcal{J}m_i$, $p_{i+1}\in\sigma\mathcal{J}m_{i+1}$ and $\mathcal{J}$ is monotone, we see that

$$\langle p_i, m_{i+1}-m_i\rangle \leq \langle p_{i+1}, m_{i+1}-m_i\rangle. \qquad (3.11)$$

From (3.9) and (3.10), we obtain

$$
\begin{aligned}
&2\langle p_i, m_{i+1}-n_i\rangle + 2\sigma\langle \mathcal{K}n_i, e-n_i\rangle + 2\langle p_{i+1}, e-m_{i+1}\rangle\\
&\leq 2\langle p_i, m_{i+1}-n_i\rangle + 2\sigma\langle \mathcal{K}e, e-n_i\rangle + 2\sigma\langle \mathcal{K}e, m_{i+1}-e\rangle\\
&= 2\langle p_i+\sigma\mathcal{K}e, m_{i+1}-n_i\rangle\\
&= 2\langle p_i+\sigma\mathcal{K}e, m_{i+1}-m_i\rangle - 2\langle p_i+\sigma\mathcal{K}e, m_i-m_{i-1}\rangle\\
&\leq 2\langle p_{i+1}+\sigma\mathcal{K}e, m_{i+1}-m_i\rangle - 2\langle p_i+\sigma\mathcal{K}e, m_i-m_{i-1}\rangle, \qquad (3.12)
\end{aligned}
$$

where the last equality follow from $n_i=2m_i-m_{i-1}$, while the last inequality is from (3.11).
By incorporating (3.6), (3.7), (3.8) and (3.12) into (3.5), the following result is obtained:

$$0 \leq \frac{1}{1+\varrho}\|m_{i+1}-m_i\|^2 - (\frac{1}{1+\varrho}-\frac{\epsilon\varrho^2}{(1+\varrho)^2})\|m_{i+1}-n_i\|^2 - \frac{1}{1+\varrho}\|m_i-n_i\|^2 + \frac{1}{1+\varrho}\|m_i-e\|^2$$

$$+\frac{\varrho^2}{\epsilon(1+\varrho)^2}\|m_i-q_{i-1}\|^2+\frac{\varrho}{1+\varrho}\|q_i-e\|^2-\frac{\varrho}{(1+\varrho)^2}\|m_i-q_i\|^2-\|m_{i+1}-e\|^2-\frac{1}{1+\varrho}\|m_{i+1}-m_i\|^2$$
$$+\frac{\varrho}{(1+\varrho)^2}\|q_i-m_i\|^2+\sigma\mathcal{L}(1+\sqrt{2})\|n_i-m_i\|^2+\sigma\mathcal{L}\|m_i-n_{i-1}\|^2+\sqrt{2}\sigma\mathcal{L}\|m_{i+1}-n_i\|^2$$
$$+2\langle p_{i+1}+\sigma\mathcal{K}e,m_{i+1}-m_i\rangle-2\langle p_i+\sigma\mathcal{K}e,m_i-m_{i-1}\rangle.$$

This implies

$$\begin{aligned}\|m_{i+1}-e\|^2 \le\ & \frac{1}{1+\varrho}\|m_{i+1}-m_i\|^2-(\frac{1}{1+\varrho}-\frac{\epsilon\varrho^2}{(1+\varrho)^2})\|m_{i+1}-n_i\|^2-\frac{1}{1+\varrho}\|m_i-n_i\|^2+\frac{1}{1+\varrho}\|m_i-e\|^2\\ &+\frac{\varrho^2}{\epsilon(1+\varrho)^2}\|m_i-q_{i-1}\|^2+\frac{\varrho}{1+\varrho}\|q_i-e\|^2-\frac{\varrho}{(1+\varrho)^2}\|m_i-q_i\|^2-\frac{1}{1+\varrho}\|m_{i+1}-m_i\|^2\\ &+\frac{\varrho}{(1+\varrho)^2}\|q_i-m_i\|^2+\sigma\mathcal{L}(1+\sqrt{2})\|n_i-m_i\|^2+\sigma\mathcal{L}\|m_i-n_{i-1}\|^2+\sqrt{2}\sigma\mathcal{L}\|m_{i+1}-n_i\|^2\\ &-\|p_{i+1}+\sigma\mathcal{K}e\|^2-\|m_{i+1}-m_i\|^2+\|p_{i+1}+\sigma\mathcal{K}e+m_{i+1}-m_i\|^2\\ &+\|p_i+\sigma\mathcal{K}e\|^2+\|m_i-m_{i-1}\|^2-\|p_i+\sigma\mathcal{K}e+m_i-m_{i-1}\|^2. \end{aligned}\tag{3.13}$$

Now, similar to (3.7), we obtain

$$\varrho\|q_{i+1}-e\|^2=\frac{\varrho}{1+\varrho}\|m_{i+1}-e\|^2+\frac{\varrho^2}{1+\varrho}\|q_i-e\|^2-\frac{\varrho^2}{(1+\varrho)^2}\|m_{i+1}-q_i\|^2.\tag{3.14}$$

Adding (3.13) and (3.14), gives

$$\begin{aligned}&\|m_{i+1}-e\|^2+\varrho\|q_{i+1}-e\|^2\\ \le\ & \frac{1}{1+\varrho}\|m_{i+1}-m_i\|^2-(\frac{1}{1+\varrho}-\frac{\epsilon\varrho^2}{(1+\varrho)^2})\|m_{i+1}-n_i\|^2-\frac{1}{1+\varrho}\|m_i-n_i\|^2+\frac{1}{1+\varrho}\|m_i-e\|^2\\ &+\frac{\varrho^2}{\epsilon(1+\varrho)^2}\|m_i-q_{i-1}\|^2+\frac{\varrho}{1+\varrho}\|q_i-e\|^2-\frac{\varrho}{(1+\varrho)^2}\|m_i-q_i\|^2-\frac{1}{1+\varrho}\|m_{i+1}-m_i\|^2\\ &+\frac{\varrho}{(1+\varrho)^2}\|q_i-m_i\|^2+\sigma\mathcal{L}(1+\sqrt{2})\|n_i-m_i\|^2+\sigma\mathcal{L}\|m_i-n_{i-1}\|^2+\sqrt{2}\sigma\mathcal{L}\|m_{i+1}-n_i\|^2\\ &-\|p_{i+1}+\sigma\mathcal{K}e\|^2-\|m_{i+1}-m_i\|^2+\|p_{i+1}+\sigma\mathcal{K}e+m_{i+1}-m_i\|^2\\ &+\|p_i+\sigma\mathcal{K}e\|^2+\|m_i-m_{i-1}\|^2-\|p_i+\sigma\mathcal{K}e+m_i-m_{i-1}\|^2\\ &+\frac{\varrho}{1+\varrho}\|m_{i+1}-e\|^2+\frac{\varrho^2}{1+\varrho}\|q_i-e\|^2-\frac{\varrho^2}{(1+\varrho)^2}\|m_{i+1}-q_i\|^2\\ =\ & \frac{1}{1+\varrho}\|m_i-e\|^2+\varrho\|q_i-e\|^2+\sigma\mathcal{L}(1+\sqrt{2})\|n_i-m_i\|^2+\sigma\mathcal{L}\|m_i-n_{i-1}\|^2+\sqrt{2}\sigma\mathcal{L}\|m_{i+1}-n_i\|^2\\ &-\left(\frac{1}{1+\varrho}+1\right)\|m_{i+1}-m_i\|^2+\|m_i-m_{i-1}\|^2+\frac{\varrho}{1+\varrho}\|m_{i+1}-e\|^2-\frac{\varrho^2}{(1+\varrho)^2}\|m_{i+1}-q_i\|^2\\ &+\frac{1}{1+\varrho}\|m_{i+1}-m_i\|^2-\left(\frac{1}{1+\varrho}-\frac{\epsilon\varrho^2}{(1+\varrho)^2}\right)\|m_{i+1}-n_i\|^2-\frac{1}{1+\varrho}\|m_i-n_i\|^2+\frac{\varrho^2}{\epsilon(1+\varrho)^2}\|m_i-q_{i-1}\|^2\\ &-\|p_{i+1}+\sigma\mathcal{K}e\|^2+\|p_{i+1}+\sigma\mathcal{K}e+m_{i+1}-m_i\|^2+\|p_i+\sigma\mathcal{K}e\|^2-\|p_i+\sigma\mathcal{K}e+m_i-m_{i-1}\|^2. \end{aligned}$$

This implies

$$\begin{aligned}&\frac{1}{1+\varrho}\|m_{i+1}-e\|^2+\varrho\|q_{i+1}-e\|^2+\frac{\varrho^2}{\epsilon(1+\varrho)^2}\|m_{i+1}-q_i\|^2+\|m_{i+1}-m_i\|^2\\ &+\sigma\mathcal{L}\|m_{i+1}-n_i\|^2+\|p_{i+1}+\sigma\mathcal{K}e\|^2-\|p_{i+1}+\sigma\mathcal{K}e+m_{i+1}-m_i\|^2\\ \le\ & \frac{1}{1+\varrho}\|m_i-e\|^2+\varrho\|q_i-e\|^2+\frac{\varrho^2}{\epsilon(1+\varrho)^2}\|m_i-q_{i-1}\|^2+\|m_i-m_{i-1}\|^2+\sigma\mathcal{L}\|m_i-n_{i-1}\|^2\\ &-\left(1-\sigma\mathcal{L}(1+\sqrt{2})-\frac{\varrho}{1+\varrho}-\frac{\epsilon\varrho^2}{(1+\varrho)^2}\right)\|m_{i+1}-n_i\|^2-\left(\frac{\varrho^2}{(1+\varrho)^2}-\frac{\varrho^2}{\epsilon(1+\varrho)^2}\right)\|m_{i+1}-q_i\|^2\\ &-\left(1-\frac{\varrho}{1+\varrho}-\sigma\mathcal{L}(1+\sqrt{2})\right)\|m_i-n_i\|^2+\|p_i+\sigma\mathcal{K}e\|^2-\|p_i+\sigma\mathcal{K}e+m_i-m_{i-1}\|^2\\ \le\ & \frac{1}{1+\varrho}\|m_i-e\|^2+\varrho\|q_i-e\|^2+\frac{\varrho^2}{\epsilon(1+\varrho)^2}\|m_i-q_{i-1}\|^2+\|m_i-m_{i-1}\|^2+\sigma\mathcal{L}\|m_i-n_{i-1}\|^2 \end{aligned}$$

$$+\|p_i+\sigma\mathcal{K}e\|^2-\|p_i+\sigma\mathcal{K}e+m_i-m_{i-1}\|^2$$
$$-\left(1-\sigma\mathcal{L}(1+\sqrt{2})-\frac{\varrho}{1+\varrho}-\frac{\epsilon\varrho^2}{(1+\varrho)^2}\right)\left[\|m_{i+1}-n_i\|^2+\|m_i-n_i\|^2\right]-\left(\frac{\epsilon-1}{\epsilon}\right)\frac{\varrho^2}{(1+\varrho)^2}\|m_{i+1}-q_i\|^2. \quad \square$$

Theorem 3.4. *Let Algorithm 3.2 generate $\{m_i\}$ and let the conditions outlined in Assumption 3.1 be met. Assume that $0 \le \varrho < \min\left\{\frac{1}{2}\sqrt{\sigma\mathcal{L}(1-4\sigma\mathcal{L})},\ \frac{1-4\sigma^2\mathcal{L}^2}{4\sigma^2\mathcal{L}^2},\ \frac{1-\sigma\mathcal{L}(1+\sqrt{2})}{\epsilon+\sigma\mathcal{L}(1+\sqrt{2})}\right\}$ and $\sigma \in (0, \frac{1}{4L})$. Then $\{m_i\}$ is weakly convergent to a point in $(\mathcal{J}+\mathcal{K})^{-1}(0)$.*

Proof. Suppose $e \in (\mathcal{J}+\mathcal{K})^{-1}(0)$. Then for all $i \ge 1$, the sequence $\{a_i\}$ defined in (3.1) is bounded below by 0.

$$\begin{aligned}
a_i &= \frac{1}{1+\varrho}\|m_i-e\|^2+\varrho\|q_i-e\|^2+\frac{\varrho^2}{\epsilon(1+\varrho)^2}\|m_i-q_{i-1}\|^2+\|m_i-m_{i-1}\|^2+\sigma\mathcal{L}\|m_i-n_{i-1}\|^2\\
&\quad+\|p_i+\sigma\mathcal{K}e\|^2-\|p_i+\sigma\mathcal{K}e+m_i-m_{i-1}\|^2\\
&\ge \frac{1}{1+\varrho}\|m_i-e\|^2+\varrho\|q_i-e\|^2+\frac{\varrho^2}{\epsilon(1+\varrho)^2}\|m_i-q_{i-1}\|^2+\|m_i-m_{i-1}\|^2+\sigma\mathcal{L}\|m_i-n_{i-1}\|^2\\
&\quad+\|p_i+\sigma\mathcal{K}e\|^2-2\|w_{i-1}-m_{i-1}\|^2-2\sigma^2\mathcal{L}^2\|n_{i-1}-e\|^2\\
&\ge \frac{1}{1+\varrho}\|m_i-e\|^2+\|m_i-m_{i-1}\|^2+\sigma\mathcal{L}\|m_i-n_{i-1}\|^2\\
&\quad-\frac{4\varrho^2}{(1+\varrho)^2}\|n_{i-1}-m_i\|^2-\frac{4\varrho^2}{(1+\varrho)^2}\|m_i-m_{i-1}\|^2-4\sigma^2\mathcal{L}^2\|n_{i-1}-m_i\|^2-4\sigma^2\mathcal{L}^2\|m_i-e\|^2\\
&\ge \left(1-\frac{\varrho}{1+\varrho}-4\sigma^2\mathcal{L}^2\right)\|m_i-e\|^2+\left(1-\frac{4\varrho^2}{(1+\varrho)^2}\right)\|m_i-m_{i-1}\|^2\\
&\quad+\left(\sigma\mathcal{L}-\frac{4\varrho^2}{(1+\varrho)^2}-4\sigma^2\mathcal{L}^2\right)\|n_{i-1}-m_i\|^2. \qquad (3.15)
\end{aligned}$$

Thus, by the condition on ϱ and σ, we see that $0 \le a_i$ for all $i \ge 1$.

Also, the condition on ϱ and σ imply that $1-\sigma\mathcal{L}(1+\sqrt{2})-\frac{\varrho}{1+\varrho}-\frac{\epsilon\varrho^2}{(1+\varrho)^2} > 0$. Therefore, Lemma 3.3 yields

$$\lim_{i\to\infty} a_i \ \text{ exists.} \qquad (3.16)$$

and

$$\lim_{i\to\infty}\|m_i-n_i\| = \lim_{i\to\infty}\|m_{i+1}-n_i\| = \lim_{i\to\infty}\|m_{i+1}-q_i\| = 0. \qquad (3.17)$$

Thus,

$$\lim_{i\to\infty}\|m_{i+1}-m_i\| = 0. \qquad (3.18)$$

Moreover, $\{a_i\}$ is bounded. Thus, by (3.15), we obtain that $\{m_i\}$ is also bounded. Hence, the boundedness of $\{n_i\}$, $\{w_i\}$ and $\{\mathcal{K}n_i-\mathcal{K}e\}$ follows. Using these facts and (3.18), one sees that

$$\lim_{i\to\infty}\langle m_{i-1}-m_i, \mathcal{K}n_{i-1}-\mathcal{K}e\rangle = 0. \qquad (3.19)$$

Now, since $w_i = \frac{1}{1+\varrho}m_i+\frac{\varrho}{1+\varrho}q_i$, we get from (3.17) and (3.18) that

$$\lim_{i\to\infty}\|w_i-m_i\| = \frac{\varrho}{1+\varrho}\lim_{i\to\infty}\|q_i-m_i\| = 0. \qquad (3.20)$$

Also,

$$\|m_{i+1}-n_i\| \le \|m_{i+1}-m_i\|+\|n_i-m_i\| \to 0,\ i\to\infty \qquad (3.21)$$

and

$$\|m_{i+1}-w_i\| \le \|m_{i+1}-m_i\|+\|m_i-w_i\| \to 0,\ i\to\infty. \qquad (3.22)$$

By (3.2) and (2.1), we obtain

$$\begin{aligned}
&\|p_i+\sigma\mathcal{K}e\|^2-\|p_i+m_i-m_{i-1}+\sigma\mathcal{K}e\|^2\\
&=\|w_{i-1}-m_i+\sigma(\mathcal{K}e-\mathcal{K}n_{i-1})\|^2-\|w_{i-1}-m_{i-1}+\sigma(\mathcal{K}e-\mathcal{K}n_{i-1})\|^2\\
&=\|w_{i-1}-m_i\|^2-\|w_{i-1}-m_{i-1}\|^2+2\sigma\langle m_{i-1}-m_i, \mathcal{K}n_{i-1}-\mathcal{K}e\rangle\\
&\quad\to 0,\ i\to\infty \text{ (by (3.22), (3.20) and (3.19)).} \qquad (3.23)
\end{aligned}$$

Since $\{m_i\}$ is bounded, there exists $\{m_{i_k}\} \subset \{m_i\}$ such that $m_{i_k} \rightharpoonup p \in \mathcal{V}$.

Again, by (3.22) and (3.21), we see that

$$w_{i_k}-m_{i_k+1}-\sigma\mathcal{K}n_{i_k}+\sigma\mathcal{K}m_{i_k+1} \to 0,\ k\to\infty. \qquad (3.24)$$

Table 1
Description of parameters and variables in the model (4.1).

Symbol	Description
$N(t)$	Number of lung tissue cancer cells at time t (cells)
$I(t)$	Number of immune cells in lung tissue at time t (cells)
$P(t)$	Number of cancer cells spread to other parts at time t (cells)
λ	Growth rate of lung cancer cells (cells/day)
K	Carrying capacity of lung tissue (cells)
μ	Rate of cancer cell spread from lung tissue (cells/day)
σ	Rate of cancer cell spread in lung tissue (cells/day)
δ	Rate of death of spread cancer cells (cells/day)
β_1	Interaction: cancer cells and immune cells (1/day)
β_2	Interaction: immune cells and cancer cell growth (1/day)
β_3	Interaction: blood vessels and cancer cells (1/day)
φ_1, φ_2, φ_3	Effects of growth factors (1/day)

Note that

$$w_{i_k} - m_{i_k+1} - \sigma\mathcal{K}n_{i_k} + \sigma\mathcal{K}m_{i_k+1} = p_{i_k+1} + \sigma\mathcal{K}m_{i_k+1} \in \sigma(\mathcal{J}+\mathcal{K})m_{i_k+1}. \tag{3.25}$$

The graph of $\mathcal{J}+\mathcal{K}$ is closed in the space $\mathcal{V}^{\text{strong}} \times \mathcal{V}^{\text{weak}}$ since it is maximal monotone. Thus, by (3.24) and (3.25), one gets $p \in (\mathcal{J}+\mathcal{K})^{-1}(0)$.

We now show that $m_i \rightharpoonup p$. Now, set

$$b_i := -\left(\frac{\varrho^2}{\epsilon(1+\varrho)^2}\|m_i - q_{i-1}\|^2 + \|m_i - m_{i-1}\|^2 + \sigma\mathcal{L}\|m_i - n_{i-1}\|^2 + \|p_i + \sigma\mathcal{K}e\|^2 - \|p_i + \sigma\mathcal{K}e + m_i - m_{i-1}\|^2\right)$$

and

$$c_i := 2\langle m_i - q_i, q_i - e\rangle + \|m_i - q_i\|^2.$$

Thus,

$$\begin{aligned} a_i + b_i + \varrho c_i &= \frac{1}{1+\varrho}\|m_i - e\|^2 + \varrho\|q_i - e\|^2 + 2\varrho\langle m_i - q_i, q_i - e\rangle + \varrho\|m_i - q_i\|^2 \\ &= \frac{1}{1+\varrho}\|m_i - e\|^2 + \varrho\|q_i - e\|^2 + \varrho\|m_i - e\|^2 - \varrho\|m_i - q_i\|^2 - \varrho\|q_i - e\|^2 + \varrho\|m_i - q_i\|^2. \end{aligned}$$

This together with (3.16), (3.17), (3.18), (3.21) and (3.23) imply that

$$\lim_{i\to\infty}\left(\frac{1}{1+\varrho} + \varrho\right)\|m_i - e\|^2 = \lim_{i\to\infty}(a_i + b_i + \varrho c_i) \text{ exists.}$$

Hence, $\lim_{i\to\infty}\|m_i - e\|$ exists for each $e \in (\mathcal{J}+\mathcal{K})^{-1}(0)$. Therefore, by Lemma 2.3, we can infer that the sequence $\{m_i\}$ is weakly convergent to an element in $(\mathcal{J}+\mathcal{K})^{-1}(0)$. □

4. Numerical experiments

To better understand the procedure of Algorithm 3.2, let us look at a biological system in the form of fractional-order differential dynamics given in (4.1) and depicted in Fig. 1 that describes lung cancer dynamics with a focus on epithelial cells, oncogenes, tumor suppressor genes, immune cells, blood vessels, and growth factors.

$$\begin{aligned} {}_0^c\mathcal{D}_t^\gamma N(t) &= \lambda N(t)\left(1 - \frac{N(t)}{K}\right) - \mu N(t)P(t) - \beta_1 N(t)I(t), \\ {}_0^c\mathcal{D}_t^\gamma I(t) &= \varphi_1 I_0 + \varphi_2 N^2(t) - \varphi_3 I(t) - \beta_2 I(t)P(t), \\ {}_0^c\mathcal{D}_t^\gamma P(t) &= \sigma N(t)P(t) - \delta P(t) - \beta_3 I(t)P(t), \end{aligned} \tag{4.1}$$

subject to the starting assumptions specified below:

$$N(0) = N_0 > 0, \quad I(0) = I_0 > 0, \quad P(0) = P_0 > 0,$$

where ${}_0^c\mathcal{D}_t^\gamma(.)$ is the Caputo fractional derivative operator (see Definition 2.1). System (4.1) is defined with each parameters and variables assumed to be non-negative. We take $N(t)$ as the population of cancer cells confined to the lung tissue at time t, $P(t)$ denotes the count of cancer cells metastasized to distant areas within the body, and $I(t)$ quantifies the immune cells present within the lung tissue (see Table 1).

The dynamics of the system account for the influence of oncogenes and tumor suppressor genes, represented by the cancer cell growth rate, λ, and the tissue's carrying capacity, K. Interactions with immune cells are modeled through the parameter β_1, while the growth and dissemination of cancer cells are influenced by parameters μ, σ, and δ. Additionally, the model incorporates the impact

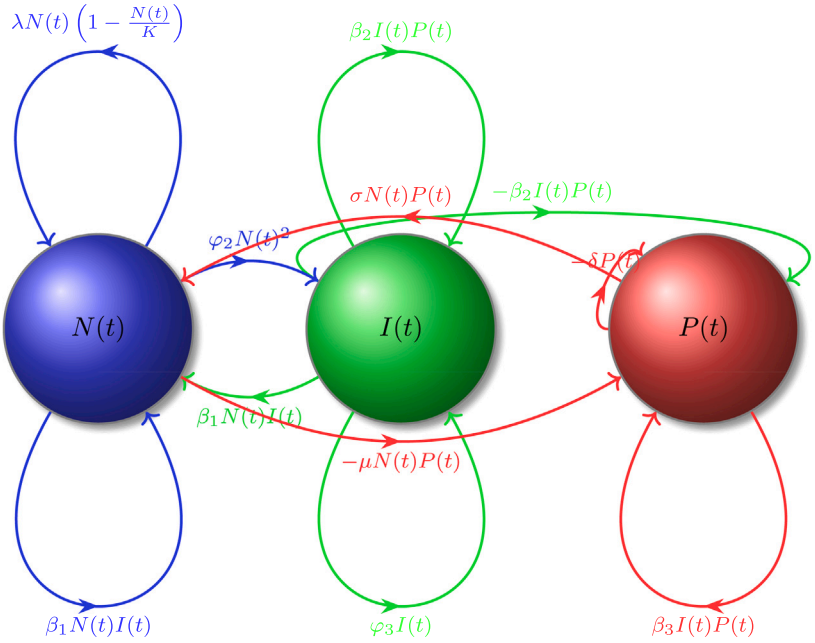

Fig. 1. Diagrammatic representation of the fractional-order lung cancer model in (4.1).

of blood vessels on nutrient delivery and metastasis promotion via the parameter β_3. The concentration of growth factors is given by parameters φ_1, φ_2, and φ_3, which together indicate the degree of their contribution in inducing and sustaining tumor growth. The first equation in system (4.1) models the population of cancer cells in the lung tissue denoted as $N(t)$. This equation portrays the processes of division of cells with cancer, their contact with the immune system, and balance with the actions of growth factor and other biological factors. The expression $\lambda N(t)\cdot(1-\frac{N(t)}{K})$ describes the growth of these cancer cells, λ representing lung cancer growth rate and K the lung tissue carrying capacity. This expression takes care of the exponential growth curve of cancer cells in a tissue beyond its carrying capacity which is a natural growth pattern of the tumor. The expression $\mu N(t)P(t)$ exposes the network of cells, deprived of nutrients and oxygen, stressed by migration from lung tissue to the rest of the body. This interaction depicts the communication of cancer cells with the immune system and its function in suppressing tumor advancement and dissemination. The pro-immune term $-\beta_1 N(t)I(t)$ describes the relationship between tumor cells and the body's immune response system with the constant β_1 being the interaction rate. Such terms depict the effect cancer cells have on the immune system and vice versa which determines the growth and metastasis of cancer. The equation represented by $I(t)$ where the t denotes time is the concentration of the immune response in lung tissue as mentioned earlier. This equation depicts the dimension of immune cells, cancer cells and other biological elements governing the immune response in therapeutic conditions. The term $\varphi_1 I_0 + \varphi_2 N^2(t)$ include effects of enhancing factors and immunity cells where the two factors interact with growing metastatic cancer cells. The parameter φ_1 and φ_2 represents enhancing factors and immunity cells towards the development of cancer cells respectively. This term describes the impact of microenvironmental inputs on the proliferation and reproduction of metastatic tumor cells. The coefficient, $-\varphi_3 I(t)$, indicates the limiting influence on the proliferation of metastatic tumor cells by growth factor concentrations. Also, φ_3 refers to the impairment of metastatic cancer cell proliferation via growth factors. This term encapsulates the intricate interactions involved in regulating the proliferation of cancer cells and their spread. The term $-\beta_2 P(t)I(t)$ incorporates the effect of the immune system on metastatic cancer cells. Here, β_2 denotes the dynamical rate between the body's immune cells and cancerous cells. This term depicts the effect of the immune system on the proliferation and metastasis of cancer cells other than the primary site. The third equation system (4.1) illustrates the process of cancer cells which metastasize in other regions of the body, and is represented by $P(t)$. This enumeration focuses on the factors responsible for the proliferation and the metastasis of the cancerous cells other than the lung tissues. The term $\sigma N(t)P(t)$ describes this process, with $N(t)$ depicting population of the tumor cells within the lung tissue that are spreading throughout the body at a rate σ. In simple words, this term describes the activity of immune cells in the targeting and engagement with cancer cells, and thus determines the evolution and dissemination of the cancer. The deceased cancerous cells transform into this term $-\delta P(t)$, whereas the variable δ identifies the death of spread cells. The term $-\beta_3 P(t)I(t)$ considers the influence of the vascular system on the position of the immune cells within the tumor and its possible interactions. Here, an interaction rate β_3 exists between the blood vessels and the cancer cells. This interaction is fundamental to the process of tumor angiogenesis, whereby new capillaries are formed to provide nutrients and oxygen to cancer cells, thus promoting the expansion and spread of the tumor.

Fractional-order differential equations have emerged as a powerful tool for modeling intricate systems, surpassing the capabilities of conventional integer-order frameworks. Their applications extend across disciplines such as the fractional order conception,

which delivers improved accuracy while tracking intricate non-linear behaviors commonly found in biological processes like lung cancer dynamics [29,30]. This is because attention deficit models are fractional order capacity models and it is expected that they have memory hence why a model for this order would be able to integrate past states and events that are very important in the development of the disease. These also allow a greater flexibility to describe the complex interactions occurring among various components of the biological system in fractional-order models. Also, fractional-order derivatives enabled the representation of fractional-order kinetics, thus allowing more close-to-reality modeling for processes such as cell proliferation, migration, and interactions among the cancerous cells, the immune cells, and various elements within the cancerous microenvironment. Another advantage of fractional-order models is the robustness with which they handle uncertainties and variability inherent in biological systems [31,32]. The fractional-order framework is able to catch the intrinsic variability and heterogeneity evident in biological data, allowing for a richer and more reliable illustration of lung cancer dynamics. It enhances the predictive capability of the model and extends the generality towards different experimental conditions and various patient populations. In this regard, incorporating fractional-order dynamics in the model indeed provides an added level of sophistication for representing lung cancer dynamics with enhanced realism. It affords a window into basic causative mechanisms underlying the growth and dissemination of a tumor and host-immune response, further ensuring treatment outcomes optimized to the characteristics unique to a given patient.

4.1. Analysis of existence and uniqueness of solutions for system (4.1)

We rewrite system (4.1) as

$$ {}_0^c D_t^\gamma X(t) = \mathcal{K}_1 X(t) + N(t)\mathcal{K}_2 X(t) + I(t)\mathcal{K}_3 X(t) + P(t)\mathcal{K}_4 X(t) + S, \quad X(0) = X_0, \tag{4.2} $$

where

$$ X(t) = \begin{pmatrix} N(t) \\ I(t) \\ P(t) \end{pmatrix}, \quad \mathcal{K}_1 = \begin{pmatrix} \lambda & 0 & 0 \\ 0 & -\varphi_3 & 0 \\ 0 & 0 & -\delta \end{pmatrix}, \quad \mathcal{K}_2 = \begin{pmatrix} -\frac{\lambda}{K} & 0 & 0 \\ \varphi_2 & 0 & 0 \\ 0 & 0 & \sigma \end{pmatrix} $$

$$ \mathcal{K}_3 = \begin{pmatrix} -\beta_1 & 0 & 0 \\ 0 & 0 & -\beta_2 \\ 0 & 0 & 0 \end{pmatrix}, \quad \mathcal{K}_4 = \begin{pmatrix} -\mu & 0 & 0 \\ 0 & 0 & -\beta_2 \\ 0 & -\beta_3 & 0 \end{pmatrix}, \quad S = \begin{pmatrix} 0 \\ \varphi_1 I_0 \\ 0 \end{pmatrix}. $$

Theorem 4.1. *$X \in C^*[0,\tau]$ is the unique solution of System (4.2).*

Proof. We can apply the Riemann–Liouville fractional integral (Definition 2.2) to get

$$ \begin{aligned} X(t) = X(0) &+ \frac{1}{\Gamma(\gamma)} \int_0^t (t-s)^{\gamma-1} \Big(\mathcal{K}_1 X(s) + N(s)\mathcal{K}_2 X(s) + I(s)\mathcal{K}_3 X(s) \\ &+ P(s)\mathcal{K}_4 X(s) + S \Big)\, ds. \end{aligned} \tag{4.3} $$

We proceed by defining $G : C^*[0,\tau] \to C^*[0,\tau]$ as follows

$$ \begin{aligned} GX(t) = X_0 &+ \frac{1}{\Gamma(\gamma)} \int_0^t (t-s)^{\gamma-1} \Big(\mathcal{K}_1 X(s) + N(s)\mathcal{K}_2 X(s) + I(s)\mathcal{K}_3 X(s) \\ &+ P(s)\mathcal{K}_4 X(s) + S \Big)\, ds. \end{aligned} $$

Thus,

$$ \begin{aligned} e^{-Lt}(GX - GY) &= e^{-Lt} \Big[\frac{1}{\Gamma(\gamma)} \int_0^t (t-s)^{\gamma-1} \Big(\mathcal{K}_1 \Big(X(s) - Y(s) \Big) \\ &+ N(t)\mathcal{K}_2 \Big(X(s) - Y(s) \Big) + I(s)\mathcal{K}_3 \Big(X(s) - Y(s) \Big) \\ &+ P(t)\mathcal{K}_4 \Big(X(s) - Y(s) \Big)) \Big] \\ &\le \frac{1}{\Gamma(\gamma)} \int_0^t (t-s)^{\gamma-1} e^{-L(t-s)} \Big(X(s) - Y(s) \Big) \\ &\times e^{-Ls} \Big(\mathcal{K}_1 + p\mathcal{K}_2 + r\mathcal{K}_3 + s\mathcal{K}_4 \Big) ds, \end{aligned} $$

where p, r, and s represent the peak values of $N(t), I(t)$, and $P(t)$. Thus,

$$ \|e^{-Lt}(GX - GY)\| \le \Big| L^{-\gamma} \Big(\mathcal{K}_1 + p\mathcal{K}_2 + r\mathcal{K}_3 + s\mathcal{K}_4 \Big) \Big| \, \|X - Y\| \, \Big\| \frac{1}{\Gamma(\gamma)} \int_0^t s^{\gamma-1} ds \Big\|. $$

Hence,

$$ \|GX - GY\| \le \frac{\tau^\gamma}{\Gamma(\gamma+1)} \Big| L^{-\gamma} \Big(\mathcal{K}_1 + p\mathcal{K}_2 + r\mathcal{K}_3 + s\mathcal{K}_4 \Big) \Big| \, \|X - Y\|. $$

Now, if we choose L such that $\|L^\gamma\| > \frac{\tau^\gamma}{\Gamma(\gamma+1)}|\mathcal{K}_1 + p\mathcal{K}_2 + r\mathcal{K}_3 + s\mathcal{K}_4|$, then

$$\|GX - GY\| \leq \kappa\|X - Y\|,$$

where $\kappa = \frac{\tau^\gamma}{\Gamma(\gamma+1)}\left|L^{-\gamma}\left(\mathcal{K}_1 + p\mathcal{K}_2 + r\mathcal{K}_3 + s\mathcal{K}_4\right)\right| < 1$, ensuring that G is a contraction. By the Banach contraction mapping principle, G possesses a unique fixed point. Consequently, (4.3) admits a unique solution $X \in C^*[0,\tau]$. Given that (4.3) is equivalent to a Volterra integral equation and, in turn, to system (4.2), we deduce that the unique solution $X \in C^*[0,\tau]$ also solves system (4.2) uniquely within the same functional space. □

4.2. Implementation

To implement Algorithm 3.2 to solve the biological model in (4.1), we can rewrite the model as

$$ {}_0^c D_t^\gamma X(t) = f(t,\ X(t)), \quad X(0) = X_0, \tag{4.4}$$

where $X(t) = (N(t), I(t), P(t))^T$ and $f : [0,+\infty)\times\mathcal{V} \to \mathcal{V}$ is defined by

$$f(t,\ X(t)) = \mathcal{K}_1 X(t) + N(t)\mathcal{K}_2 X(t) + I(t)\mathcal{K}_3 X(t) + P(t)\mathcal{K}_4 X(t) + S, \tag{4.5}$$

$\mathcal{K}_1, \mathcal{K}_2, \mathcal{K}_3, \mathcal{K}_4$ and S are as defined in (4.2).

Equivalently,

$$f(t,\ X(t)) = \begin{pmatrix} \lambda N(t)\left(1 - \frac{N(t)}{K}\right) - \mu N(t)P(t) - \beta_1 N(t)I(t) \\ \varphi_1 I_0 + \varphi_2 N^2(t) - \varphi_3 I(t) - \beta_2 I(t)P(t) \\ \sigma N(t)P(t) - \delta P(t) - \beta_3 I(t)P(t) \end{pmatrix}. \tag{4.6}$$

Theorem 4.2. *The fractional-order lung cancer model in system (4.1) is a monotone inclusion problem of the form:*

$$0 \in f(X(t)) + N_C(X(t)),$$

where f is monotone and Lipschitz continuous and N_C is the normal cone to C, which is maximal monotone.

Proof. At equilibrium (${}_0^c D_t^\gamma X(t) = 0$), we have $0 = f(X(t))$.

We now decompose $f = J + K$, and define the convex potential:

$$h(X(t)) = \frac{\lambda}{2}N^2(t)\left(1 - \frac{N(t)}{K}\right) - \frac{\varphi_3}{2}I^2 - \frac{\delta}{2}P^2(t).$$

We denote the gradient ∇h by J:

$$J(X(t)) = \begin{pmatrix} \lambda N\left(1 - \frac{N}{K}\right) \\ -\varphi_3 I \\ -\delta P \end{pmatrix}.$$

Since h is convex for $\lambda, \varphi_3, \delta \geq 0$, $J = \nabla h$ is monotone by Rockafellar's theorem.

The remaining terms in f form $K(X(t))$:

$$K(X(t)) = \begin{pmatrix} -\mu N(t)P(t) - \beta_1 N(t)I(t) \\ \varphi_1 I_0 + \varphi_2 N^2(t) - \beta_2 I(t)P(t) \\ \sigma N(t)P(t) - \beta_3 I(t)P(t) \end{pmatrix}.$$

The Jacobian $\widehat{J}_K$ is:

$$\widehat{J}_K(X(t)) = \begin{pmatrix} -\mu P(t) - \beta_1 I(t) & -\beta_1 N(t) & -\mu N(t) \\ 2\varphi_2 N(t) & -\beta_2 P(t) & -\beta_2 I(t) \\ \sigma P(t) & -\beta_3 P(t) & \sigma N(t) - \beta_3 I(t) \end{pmatrix}.$$

For the monotonicity of K, we require $\widehat{J}_K + \widehat{J}_K^T \geq 0$. The symmetric part is:

$$\widehat{J}_K(X(t)) + \widehat{J}_K^T(X(t)) = \begin{pmatrix} -2\mu P(t) - 2\beta_1 I(t) & 2\varphi_2 N(t) - \beta_1 N(t) - \beta_3 P(t) & -\mu N(t) + \sigma P(t) \\ 2\varphi_2 N(t) - \beta_1 N(t) - \beta_3 P(t) & -2\beta_2 P(t) & -\beta_2 I(t) - \beta_3 P(t) \\ -\mu N(t) + \sigma P(t) & -\beta_2 I(t) - \beta_3 P(t) & 2\sigma N(t) - 2\beta_3 I(t) \end{pmatrix}.$$

If μ, β_i are small relative to φ_2, σ, the matrix is positive semi-definite, and thus, K is monotone. Moreover, by similar arguments as in the proof of Theorem 4.1, we can show that K and J are Lipschitz continuous. Thus, $f = J + K$ is monotone and Lipschitz continuous.

Now, note that the equilibrium condition $0 = f(X(t))$ is equivalent to the variational inequality:

$$\langle f(X), Y - X\rangle \geq 0 \quad \forall Y \in C,$$

which in turn is equivalent to the monotone inclusion:

$$0 \in f(X) + N_C(X),$$

where $N_C(X)$ is the normal cone to C at X, which is well-known to be maximal monotone. □

If we set $\mathcal{K} = f$ and $\mathcal{J} = N_C$, (1.1) simplifies into the standard variational inequality framework associated with f, and our algorithm becomes:

Algorithm 4.3. Inertial Reflected-Forward-Backward Splitting Method with Momentum for System Eq. (4.1)

Let $\sigma > 0$ and $\varrho \geq 0$. For arbitrary $m_0, m_1, q_0 \in \mathcal{V}$, let the sequence $\{m_i\}$ be generated by

$$\begin{cases} q_i = \frac{1}{1+\varrho} m_i + \frac{\varrho}{1+\varrho} q_{i-1} \\ w_i = \frac{1}{1+\varrho} m_i + \frac{\varrho}{1+\varrho} q_i \\ n_i = 2m_i - m_{i-1} \\ m_{i+1} = P_C(w_i - \sigma f n_i), \ i \geq 1. \end{cases}$$

We then apply the Riemann–Liouville integral operator (see Definition 2.2)

$${}_0^{RL}\mathcal{I}_t^{\gamma} g(t) = \frac{1}{\Gamma(\gamma)} \int_0^t (t-s)^{\gamma-1} g(s)\, ds, \quad \gamma > 0, \quad t \in [0, T_f],$$

to both sides of (4.1). So, the corresponding system will be achieved as:

$$\begin{aligned} N(t) &= N(0) + \frac{1}{\Gamma(\gamma)} \int_0^t (t-s)^{\gamma-1} \left\{ \lambda N(s)\left(1 - \frac{N(s)}{K}\right) - \mu N(s)P(s) - \beta_1 N(s)I(s) \right\} ds = f_1(N(t), I(t), P(t)), \\ I(t) &= I(0) + \frac{1}{\Gamma(\gamma)} \int_0^t (t-s)^{\gamma-1} \left\{ \varphi_1 I_0 + \varphi_2 N^2(s) - \varphi_3 I(s) - \beta_2 I(s)P(s) \right\} ds = f_2(N(t), I(t), P(t)), \\ P(t) &= P(0) + \frac{1}{\Gamma(\gamma)} \int_0^t (t-s)^{\gamma-1} \left\{ \sigma N(s)P(s) - \delta P(s) - \beta_3 I(s)P(s) \right\} ds = f_3(N(t), I(t), P(t)). \end{aligned} \tag{4.7}$$

Three steps in Algorithm 4.3 will be as follows based on system (4.7):

$$\begin{aligned} &zN_i = \tfrac{1}{1+\varrho} N_i + \tfrac{\varrho}{1+\varrho} N_{i-1}, && zP_i = \tfrac{1}{1+\varrho} P_i + \tfrac{\varrho}{1+\varrho} P_{i-1}, && zI_i = \tfrac{1}{1+\varrho} I_i + \tfrac{\varrho}{1+\varrho} I_{i-1}, \\ &wN_i = \tfrac{1}{1+\varrho} N_i + \tfrac{\varrho}{1+\varrho} zN_i, && wP_i = \tfrac{1}{1+\varrho} P_i + \tfrac{\varrho}{1+\varrho} zP_i, && wI_i = \tfrac{1}{1+\varrho} I_i + \tfrac{\varrho}{1+\varrho} zI_i, \\ &yN_i = 2N_i - N_{i-1}, && yP_i = 2P_i - P_{i-1}, && yI_i = 2I_i - I_{i-1}, \\ &N_{i+1} = P_C(wN_i - \sigma f_1 yN_i), && P_{i+1} = P_C(wP_i - \sigma f_2 yP_i), && I_{i+1} = P_C(wI_i - \sigma f_3 yI_i), \end{aligned} \tag{4.8}$$

where f_i, for $i = 1, 2, 3$, represents the right-hand side of the system described in Eq. (4.7). Before proceeding further, we discretize the equations on the right-hand side of the system (4.7). Let us assume that $h = T_f/M$ denotes the step size, and $t_i = ih$, where $i = 0, 1, \ldots, M$, are the mesh points. Now, let us examine the first equation in system (4.7) at $t = t_{i+1}$:

$$\begin{aligned} N_{i+1} &= N(0) + \frac{1}{\Gamma(\gamma)} \int_0^{t_{i+1}} (t_{i+1} - s)^{\gamma-1}\, g_1(N(s), I(s), P(s))\, ds \\ &= N(0) + \frac{1}{\Gamma(\gamma)} \sum_{m=0}^{n} \int_{t_m}^{t_{m+1}} (t_{i+1} - s)^{\gamma-1} g_1(N(s), I(s), P(s))\, ds, \end{aligned} \tag{4.9}$$

where

$$g_1(N(t), I(t), P(t)) = \lambda N(t)\left(1 - \frac{N(t)}{K}\right) - \mu N(t)P(t) - \beta_1 N(t)I(t).$$

To discretize the integral part, we use the Lagrange interpolation over the sub-interval $[t_{m-1}, t_m]$, thus we have

$$\begin{aligned} \mathcal{L}(s) &= \frac{s - t_m}{t_{m-1} - t_m} g_1(N(t_m), I(t_m), P(t_m)) + \frac{s - t_{m-1}}{t_m - t_{m-1}} g_1(N(t_{m-1}), I(t_{m-1}), P(t_{m-1})) \\ &\approx \frac{s - t_{m-1}}{h} g_{1,m} - \frac{s - t_m}{h} g_{1,m-1}, \end{aligned}$$

where $g_{1,j} = g_1(N(t_j), I(t_j), P(t_j))$. So, using integration by parts, the integral parts in (4.9) will be written as follows:

$$\begin{aligned} \int_{t_m}^{t_{m+1}} (t_{i+1} - s)^{\gamma-1} g_1(N(s), I(s), P(s))\, ds &\approx \int_{t_m}^{t_{m+1}} (t_{i+1} - s)^{\gamma-1} \frac{s - t_{m-1}}{h} g_{1,m}\, ds \\ &\quad - \int_{t_m}^{t_{m+1}} (t_{i+1} - s)^{\gamma-1} \frac{s - t_m}{h} g_{1,m-1}\, ds \\ &= \frac{h^{\gamma}}{\gamma(\gamma+1)} \left\{ (n-m)^{\gamma}(m - n - 2\gamma - 2) + (n - m + 1)^{\gamma}(n - m + \gamma + 2) \right\} g_{1,m} \end{aligned}$$

$$- \frac{h^{\gamma}}{\gamma(\gamma+1)} \left\{ (n-m)^{\gamma}(n-m+\gamma+1) - (n-m+1)^{\gamma+1} \right\} g_{1,m-1}.$$

Therefore, the formulas in the third row of (4.8) are as follows:

$$\begin{aligned} N_{i+1} = N(0) + \frac{h^{\gamma}}{\Gamma(\gamma+2)} \sum_{m=1}^{n} \Bigg[& \left\{ (n-m)^{\gamma}(m-n-2\gamma-2) + (n-m+1)^{\gamma}(n-m+\gamma+2) \right\} \times \\ & \left\{ \lambda(wN_m - \sigma y N_m)\left(1 - \frac{wN_m - \sigma y N_m}{K}\right) - \mu(wN_m - \sigma y N_m)(wP_m - \sigma y P_m) \right. \\ & \left. - \beta_1(wN_m - \sigma y N_m)(wI_m - \sigma y I_m) \right\} + \left\{ (n-m)^{\gamma}(n-m+\gamma+1) - (n-m+1)^{\gamma+1} \right\} \times \\ & \left\{ \lambda(wN_{m-1} - \sigma y N_{m-1})\left(1 - \frac{wN_{m-1} - \sigma y N_{m-1}}{K}\right) - \mu(wN_{m-1} - \sigma y N_{m-1})(wP_{m-1} - \sigma y P_{m-1}) \right. \\ & \left. - \beta_1(wN_{m-1} - \sigma y N_{m-1})(wI_{m-1} - \sigma y I_{m-1}) \right\} \Bigg], \end{aligned} \tag{4.10}$$

$$\begin{aligned} I_{i+1} = I(0) + \frac{h^{\gamma}}{\Gamma(\gamma+2)} \sum_{m=1}^{n} \Bigg[& \left\{ (n-m)^{\gamma}(m-n-2\gamma-2) + (n-m+1)^{\gamma}(n-m+\gamma+2) \right\} \times \\ & \left\{ \varphi_1 I_0 + \varphi_2(wN_m - \sigma y N_m)^2 - \varphi_3(wI_m - \sigma y I_m) - \beta_2(wI_m - \sigma y I_m)(wP_m - \sigma y P_m) \right\} \\ & + \left\{ (n-m)^{\gamma}(n-m+\gamma+1) - (n-m+1)^{\gamma+1} \right\} \left\{ \varphi_1 I_0 + \varphi_2(wN_{m-1} - \sigma y N_{m-1})^2 \right. \\ & \left. - \varphi_3(wI_{m-1} - \sigma y I_{m-1}) - \beta_2(wI_{m-1} - \sigma y I_{m-1})(wP_{m-1} - \sigma y P_{m-1}) \right\} \Bigg], \end{aligned} \tag{4.11}$$

$$\begin{aligned} P_{i+1} = P(0) + \frac{h^{\gamma}}{\Gamma(\gamma+2)} \sum_{m=1}^{n} \Bigg[& \left\{ (n-m)^{\gamma}(m-n-2\gamma-2) + (n-m+1)^{\gamma}(n-m+\gamma+2) \right\} \times \\ & \left\{ \sigma(wN_m - \sigma y N_m)(wP_m - \sigma y P_m) - \delta(wP_m - \sigma y P_m) - \beta_3(wI_m - \sigma y I_m)(wP_m - \sigma y P_m) \right\} \\ & \left\{ (n-m)^{\gamma}(n-m+\gamma+1) - (n-m+1)^{\gamma+1} \right\} \left\{ \sigma(wN_{m-1} - \sigma y N_{m-1})(wP_{m-1} - \sigma y P_{m-1}) \right. \\ & \left. - \delta(wP_{m-1} - \sigma y P_{m-1}) - \beta_3(wI_{m-1} - \sigma y I_{m-1})(wP_{m-1} - \sigma y P_{m-1}) \right\} \Bigg]. \end{aligned} \tag{4.12}$$

Values of parameters in system (4.1) and starting values are considered as follows:

$$\begin{aligned} & \lambda = 0.3, \quad K = 10, \quad \mu = 0.01, \quad \beta_1 = 0.1, \quad \beta_2 = 0.1, \quad \beta_3 = 0.4, \\ & \varphi_1 = 0.3, \quad \varphi_2 = 0.4, \quad \varphi_3 = 0.1, \quad \sigma = 0.7, \quad \delta = 0.01, \quad N(0) = 200, \\ & N(1) = 250, \quad P(0) = 2, \quad P(1) = 4, \quad I(0) = 100, \quad I(1) = 150, \quad h = 2^{-6}, \quad T_f = 10. \end{aligned}$$

Figures depicting the state variables $N(t)$, $I(t)$, and $P(t)$ are presented in Figs. 2 to 13 for various values of γ, ϱ, and σ. The surface plots in Fig. 2 depict the general dynamics of the state variables for several iterations, and these dynamics are elaborated in subsequent figures. In Fig. 3 there is a slight balance between state variables $I(t)$ and $P(t)$ while $N(t)$ decrease significantly, with fixed values of γ and ϱ ($\gamma = 0.3$, $\varrho = 0.7$). In Fig. 4, a decreasing trend is observed for $N(t)$ with $\gamma = 0.5$ and $\varrho = 0.7$. However, as σ increases, the values of $N(t)$ also increase and approach $N(t) = 100$. For $\sigma = 0.89$, the values of $I(t)$ approach $I(t) = 200$ after $t = 4$, while the values of $P(t)$ increase and approach $P(t) = 200$. Fig. 5 illustrates the decreasing behavior of $N(t)$ for $\gamma = 0.7$, $\varrho = 0.7$, and varying values of σ, with the values approaching $N(t) = 50$. After $t = 2$, the values of $I(t)$ and $P(t)$ start to increase, with $P(t)$ approaching $P(t) = 200$. In Fig. 6, a decreasing trend is depicted for $N(t)$ and $I(t)$ with $\gamma = 0.9$, $\varrho = 0.7$, and $\sigma = 0.8$, 0.81, 0.83, 0.85, 0.87. However, their values stabilize around $N(t) = 50$, $I(t) = 50$, while $P(t)$ increases and approaches $P(t) = 250$. Similar behavior is observed in Fig. 7 for the scenario with $\gamma = 0.5$, $\sigma = 0.8$, $\varrho = 0.7$, 0.71, 0.73, 0.75, 0.77, 0.79, where both $N(t)$ and $I(t)$ exhibit a decreasing trend. In Fig. 8, all plots exhibit a similar pattern: $N(t)$ decreases, while $P(t)$ and $I(t)$ increase and stabilize around $N = 150$, $P = 175$, and $I = 190$ for $\gamma = 0.3$, $\sigma = 0.9$, $\varrho = 0.75$, 0.8, 0.85, 0.9. It appears that when the values of ϱ approach $\sigma = 0.9$, the perturbation of the initial values of N, P, and I diminishes. Fig. 9 shows that all functions behave similarly with increasing values of ϱ ($\varrho = 0.75$, 0.8, 0.85, 0.9) for $\gamma = 0.9$ and $\sigma = 0.9$. Both $N(t)$ and $I(t)$ exhibit a decreasing trend, while $P(t)$ increases. In Fig. 10, the values of $N(t)$ tend to $N = 200$ with an increasing trend, $P(t)$ shows a linear behavior, and $I(t)$ decreases and stabilizes around $I = 100$ for $\gamma = 0.7$, $\varrho = 0.9$, and $\sigma = 0.9$, 0.91, 0.93, 0.95, 0.97, 0.99. Similarly, in Fig. 11, for $\gamma = 0.7$, $\sigma = 0.9$, and various values of ϱ ($\varrho = 0.9$, 0.91, 0.93, 0.95, 0.97, 0.99), both $N(t)$ and $I(t)$ decrease, while $P(t)$ increases and stabilizes around $P = 225$ after $t = 2$. Fig. 12 for $\gamma = 0.5$, $\varrho = 0.75$, $\sigma = 0.75$, the state variables of $N(t)$, $I(t)$, and $P(t)$ stabilize around $N = 80$, $P = 100$, and $I = 100$. For $\varrho = \sigma = 0.8$, 0.85, 0.9, 0.95, N decreases but approaches $N = 200$, and $P(t)$ increases. Fig. 13 illustrates the behaviors of N, P, and I for $\varrho = 0.9$, $\sigma = 0.9$, and varying values of γ ($\gamma = 0.1$, 0.3, 0.5, 0.7, 0.9, 1). In the figures, $N(t)$ decreases, $P(t)$ increases, and $I(t)$ decreases as the fractional derivative order increases.

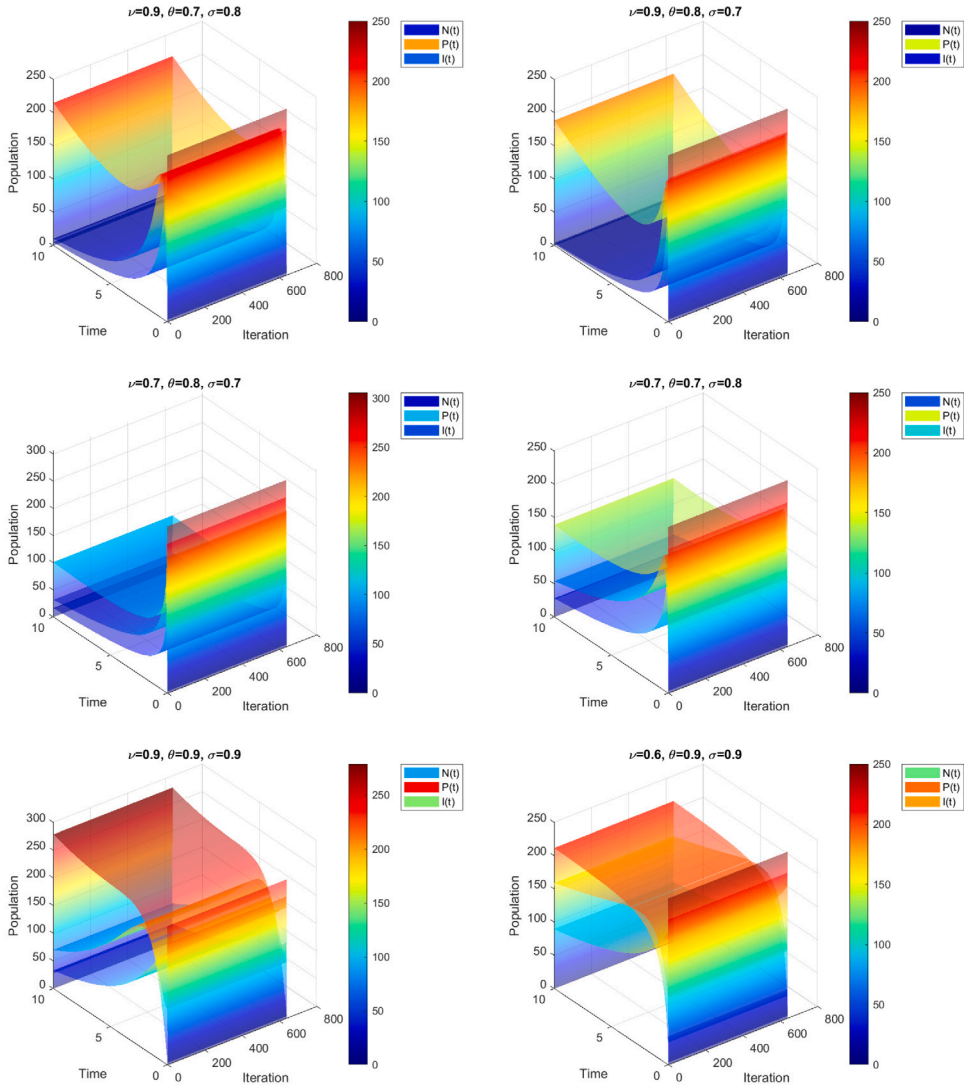

Fig. 2. Surface plots of state variables $N(t), P(t)$, and $I(t)$ for several iterations, $\gamma = 0.6, 0.9$, $\varrho = 0.7, 0.8, 0.9$ and $\sigma = 0.7, 0.8, 0.9$.

5. Result and discussion

The figures depicting the state variables $N(t)$, $I(t)$, and $P(t)$ are presented in Figs. 2–13, showcasing the dynamics under various combinations of γ, ϱ, and σ for an endemic case of the lung cancer progression, and without treatment. These figures offer insights into the behavior of the biological system described by system (4.1). By analyzing the trends and patterns exhibited by the state variables under different scenarios, we can draw meaningful conclusions about the impact of the fractional-order parameters γ, ϱ, and σ on the evolution of cancer cells ($N(t)$ and $P(t)$) and immune cells ($I(t)$) over time. We see that the choice of σ appears to be important with the dynamics of the biological system. It shows the importance of carefully choosing parameter values correctly reflecting the biological context. For $\sigma = 0.81$, the starting values of cancer cells ($N(t)$) increase, while those of immune cells ($I(t)$) decrease. This depicts a scenario where the system experiences cancer cell proliferation over immune response, which could potentially lead to disease progression and unhealthy outcomes. For $\sigma = 0.83$ the starting values of cancer cells ($N(t)$) increase, while those of immune cells ($I(t)$) decrease. This goes on to bolster the idea of an imbalance in the biological system, indicating a scenario where cancer cells may outpace the immune response, potentially leading to tumor growth and metastasis. Also, as the fractional-order operator γ increases, the gap between each state variable ($N(t), I(t), P(t)$) widens. Biologically, this indicates that past values' influence on the system's current state becomes more pronounced as γ increases. In other words, higher values of γ magnify the memory effect in the model, making the system display some deviations from its initial conditions over time. This indicates that long-term memory and past dynamics are more dominant in shaping the behavior of the biological system described by the model. The observed dynamics in the state variables $N(t)$, $I(t)$, and $P(t)$ provide important insights into the underlying

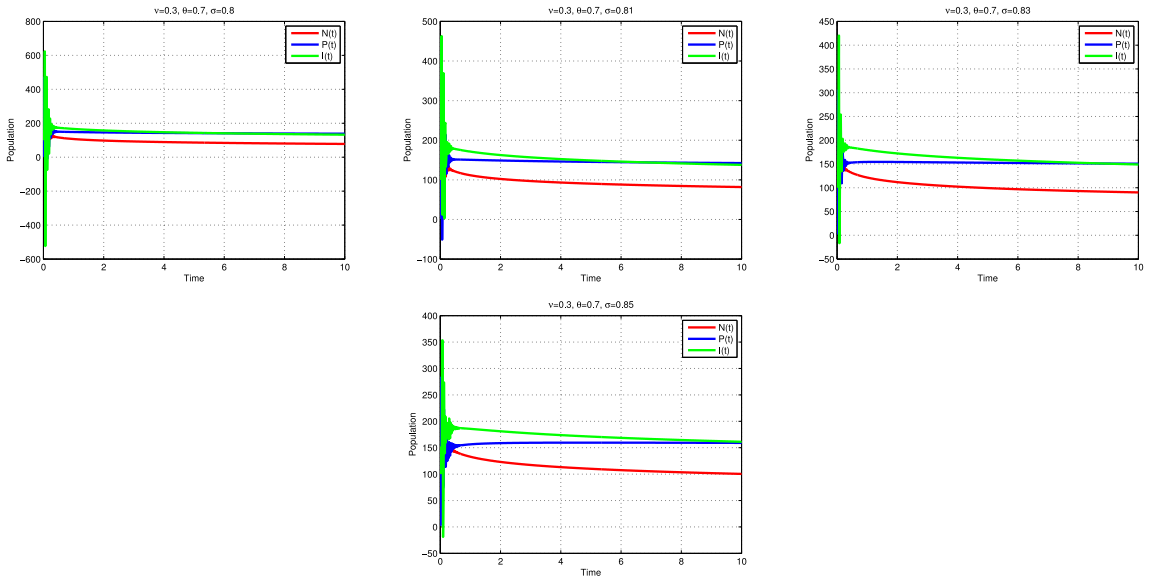

Fig. 3. Plots of state variables $N(t), P(t)$, and $I(t)$ for $\gamma = 0.3, \rho = 0.7$ and different values of σ.

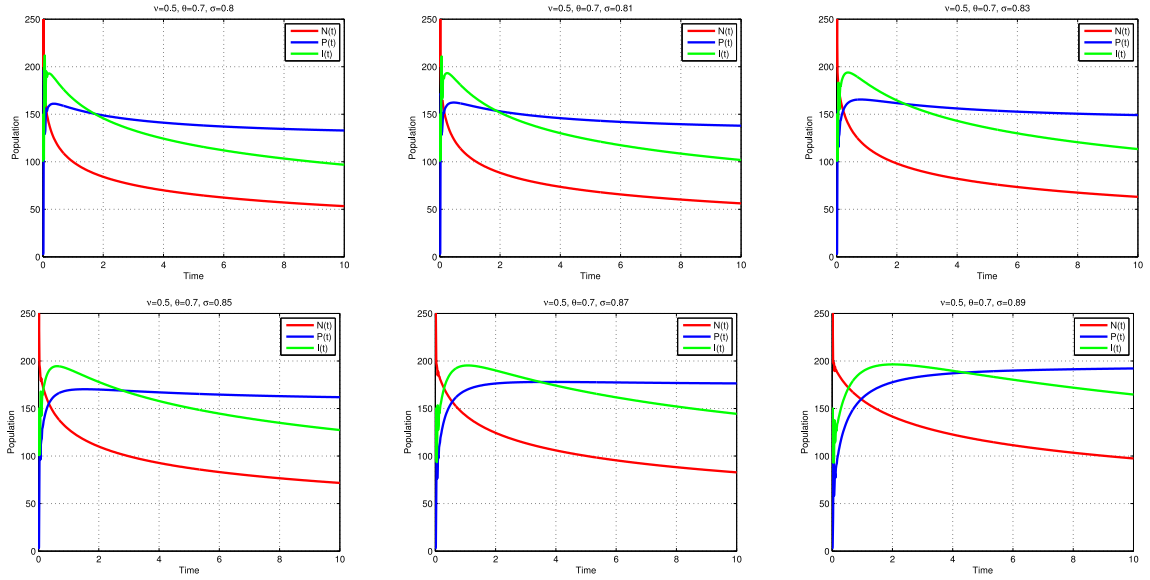

Fig. 4. Plots of state variables $N(t), P(t)$, and $I(t)$ for $\gamma = 0.5, \rho = 0.7$ and different values of σ.

biological processes of lung cancer progression and immune response. The variations in these variables under different parameter settings shed light on how the fractional order and other parameters influence the behavior of cancer cells and immune cells within the body. For instance, the stabilization of $N(t)$, $I(t)$, and $P(t)$ around certain values in Fig. 3 for $\sigma = 0.85$ suggests a balanced state where cancer cells, immune cells, and healthy cells are maintained at relatively stable levels. In Fig. 4, the increase in $N(t)$ and $P(t)$ with higher σ values indicates a scenario where cancer cell growth is favored, possibly due to reduced immune surveillance or enhanced tumor-promoting factors. Similarly, the decreasing $N(t)$ and increasing $I(t)$ observed in Fig. 5 suggest a weakening immune response against cancer cells, leading to their unchecked proliferation. The trends in Figs. 6 and 7 further underscore the complex interplay between cancer cells, immune cells, and treatment effects. For instance, the decreasing $N(t)$ and $I(t)$ coupled with increasing $P(t)$ in Fig. 6 may indicate a response to treatment where cancer cells are targeted but at the expense of immune suppression. Conversely, the decreasing $N(t)$ and $I(t)$ observed in Fig. 8 may suggest a more favorable outcome with reduced cancer cell burden and preserved immune function.

From this research, medical practitioners can get valuable knowledge related to the dynamics of lung cancer progression and the importance of different model parameters. This involves an explanation of the order γ and the parameter, σ. The order γ shows

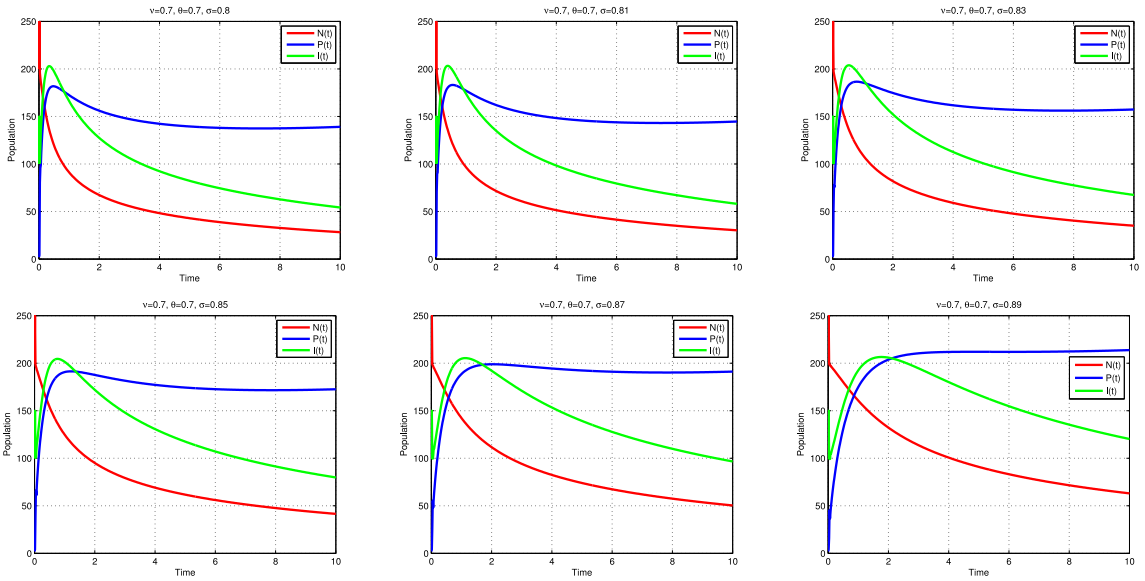

Fig. 5. Plots of state variables $N(t), P(t)$, and $I(t)$ for $\gamma = 0.7, \varrho = 0.7$ and different values of σ.

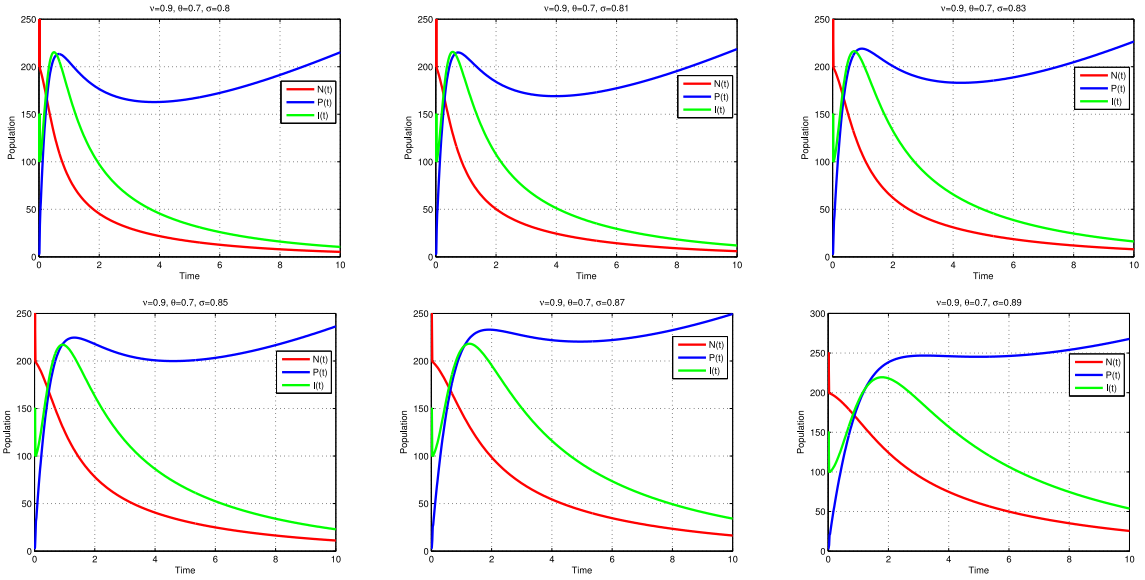

Fig. 6. Plots of state variables $N(t), P(t)$, and $I(t)$ for $\gamma = 0.9, \varrho = 0.7$ and different values of σ.

the actual degree of fractional differentiation in this model equations. It practically denotes the level at which the memory effect and non-local interactions enter into describing the dynamics of lung cancer. The higher the γ, the stronger the dependence of a current state from the past values, and consequently, the stronger the emphasis on historical data in terms of understanding disease evolution. Medical practitioners could use the information obtained from this video in formulating treatment strategies, taking into consideration both the immediate and the later dynamics of the patient's health. Along the same lines, the biological parameter σ is also very much vital in the functioning of the biological system. It determines the growth direction of the cancer cells, and their growth in relation to the immune system response. However, by carefully choosing these parameters, practitioners may visualize how the administration of various therapeutic techniques will alter the progression of the illness. As a result, this will help the practitioner determine the appropriate time and type of intervention needed to manage lung cancer. In the same way, the parameter ϱ and the algorithm presented also elicit interest from medical practitioners. The parameterϱ is an inertial term in the algorithm that controls the momentum which is directly related to convergence and stability of the numerical solution. Increasing the value of this parameter causes the volume of severance put on the momentum aspects of the algorithm leading to fast convergence speeds. Based on this information, and the factors that influence acceleration of computational simulation, medical practitioners

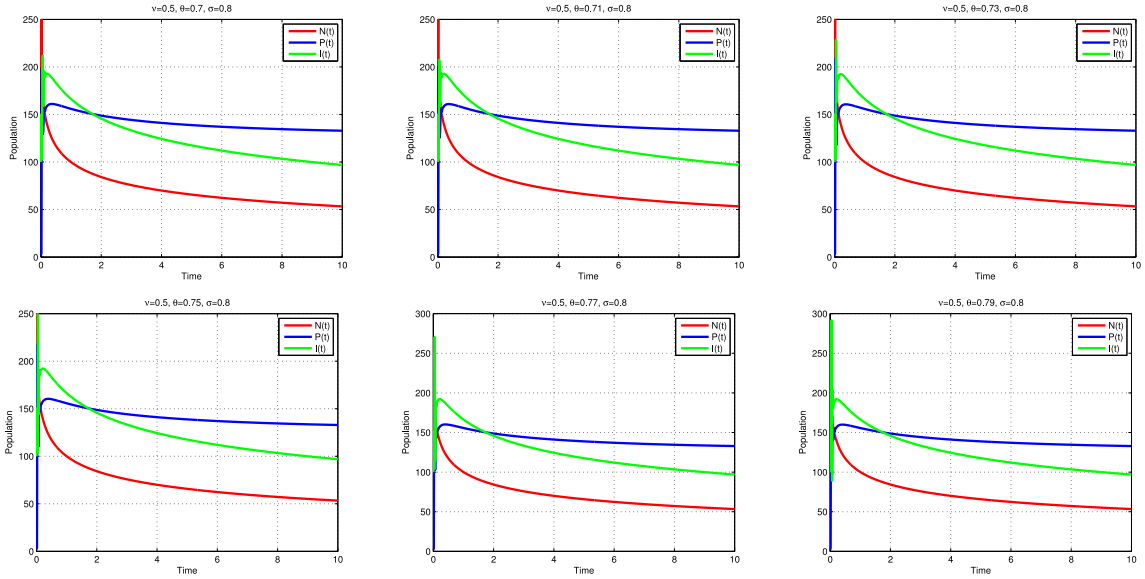

Fig. 7. Plots of state variables $N(t), P(t)$, and $I(t)$ for $\gamma = 0.5, \sigma = 0.8$ and different values of ρ.

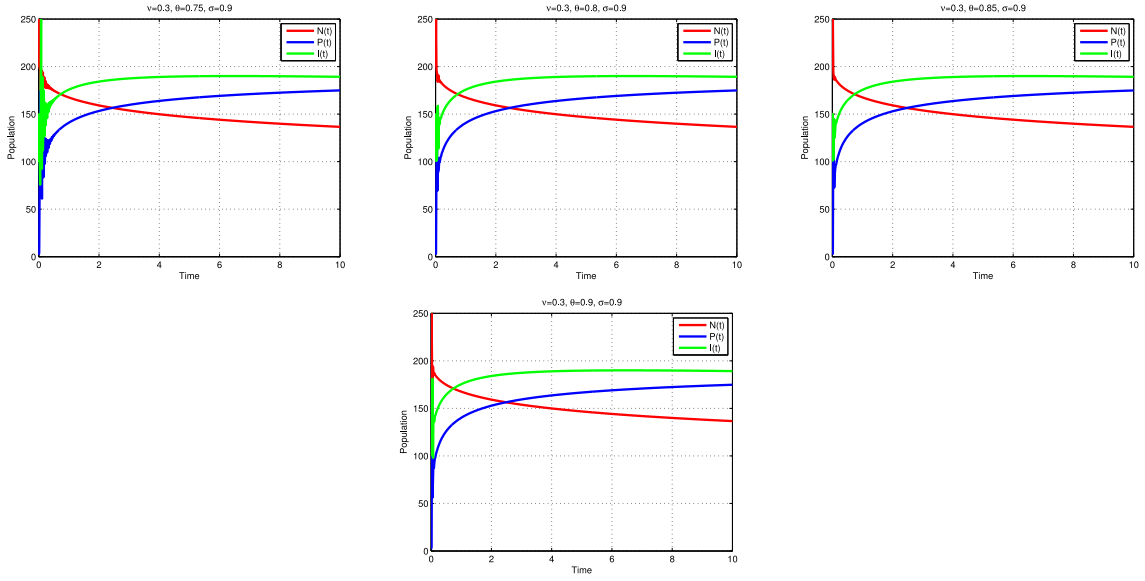

Fig. 8. Plots of state variables $N(t), P(t)$, and $I(t)$ for $\gamma = 0.3, \sigma = 0.9$ and different values of ρ.

could contribute towards establishing efficient modeling for predicting lung cancer dynamics. By understanding the effect of ρ, practitioners can choose appropriate computational parameters to get accurate and timely predictions of disease progression. An algorithm is proposed that provides a computational framework for solving a mathematical model representing the dynamics of lung cancer. With the help of the Inertial Reflected-Forward-Backward Splitting Algorithm, practitioners can simulate the variation of cancerous cells and immune cells at any instant of time. This enables the comparison of a number of treatment scenarios and the possibility to test the efficacy in the control of tumor growth and metastasis. Moreover, the efficiency of the algorithm for convergent solutions helps practitioners to accelerate analysis to generate actionable insights. It therefore helps medical practitioners to conduct computational simulations effectively, accurately analyze predictions of models, and obtain meaningful insights into clinical decision making in the management of lung cancer.

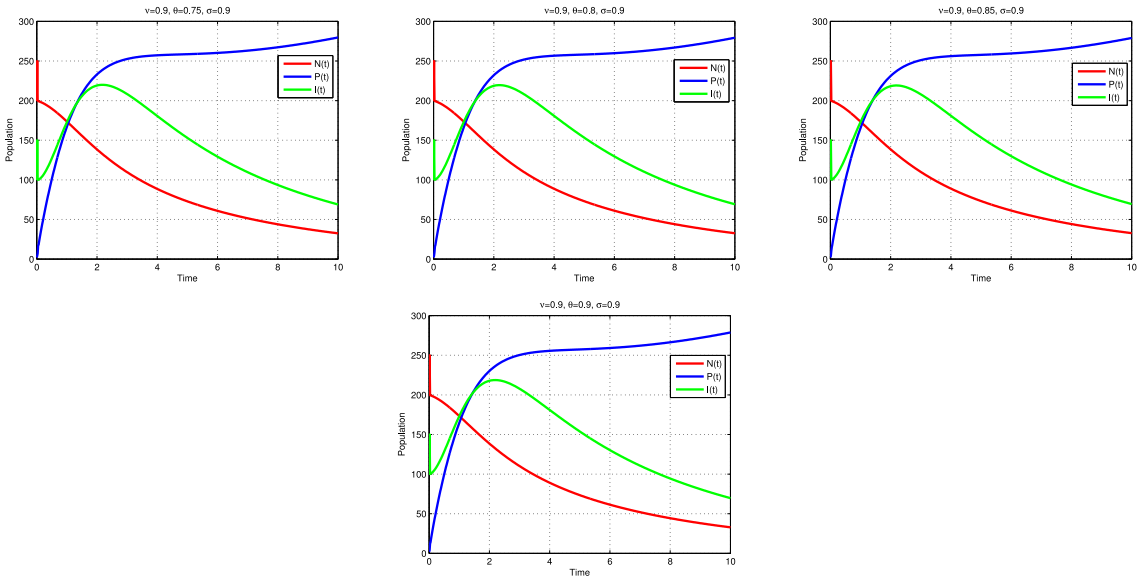

Fig. 9. Plots of state variables $N(t), P(t)$, and $I(t)$ for $\gamma = 0.9, \sigma = 0.9$ and different values of ρ.

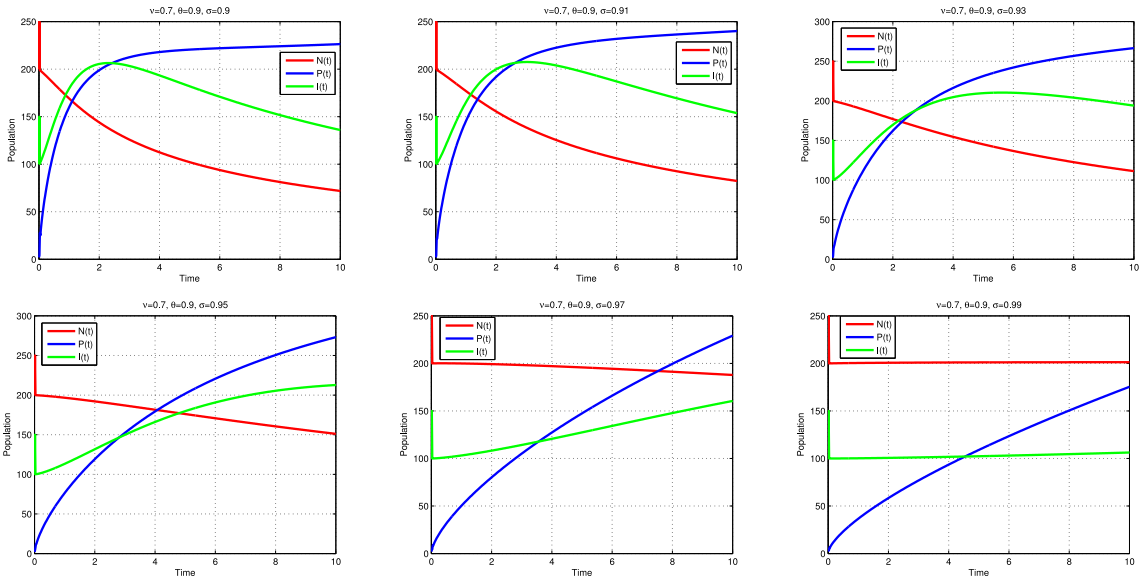

Fig. 10. Plots of state variables $N(t), P(t)$, and $I(t)$ for $\gamma = 0.7, \rho = 0.9$ and different values of σ.

6. Conclusion and future research

The reflected-forward–backward splitting method with momentum that we introduce to solve monotone inclusion problems is tests on a given fractional-order lung cancer model derived from biological process. The method finds its use in practice in the large scale and complex systems types. It provided a comprehensive computational platform for simulating and analyzing the time behavior of evolution of cancer cell and immune cells and which can be adapted to other biological models. Our results open prospects for modeling the processes of cancer development and assessing the effectiveness of treatment in the framework of fractional-order dynamics. It also has impact on the rate of search for treatment strategies, and the understanding of disease

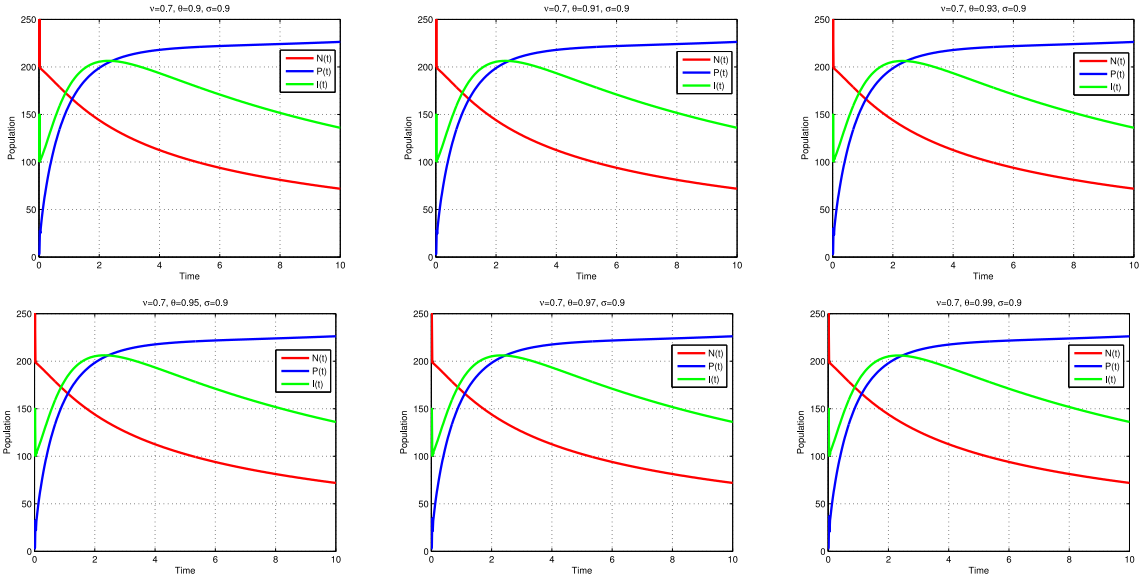

Fig. 11. Plots of state variables $N(t), P(t)$, and $I(t)$ for $\gamma = 0.7, \sigma = 0.9$ and different values of ϱ.

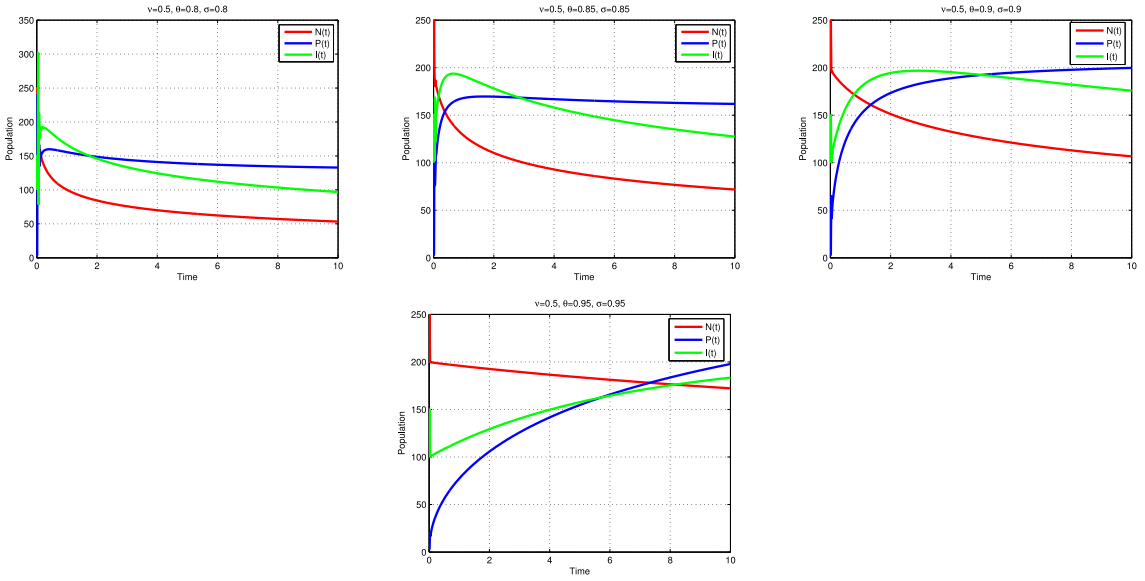

Fig. 12. Plots of state variables $N(t), P(t)$, and $I(t)$ for $\gamma = 0.5$ and different values of ϱ, σ.

dynamics to improve disease outcome in lung cancer in particular. Although, we obtained the numerical computation of the rate of convergence of our proposed algorithm in Appendix A, the theory for the rate of convergence of our proposed method will be considered in future our studies. An in-depth investigation into the method's strong and linear convergence properties would provide valuable insights. In future works, we will explore other kinds of biological modeling or additional adjustments to the algorithm's structures in response to new computational requirements.

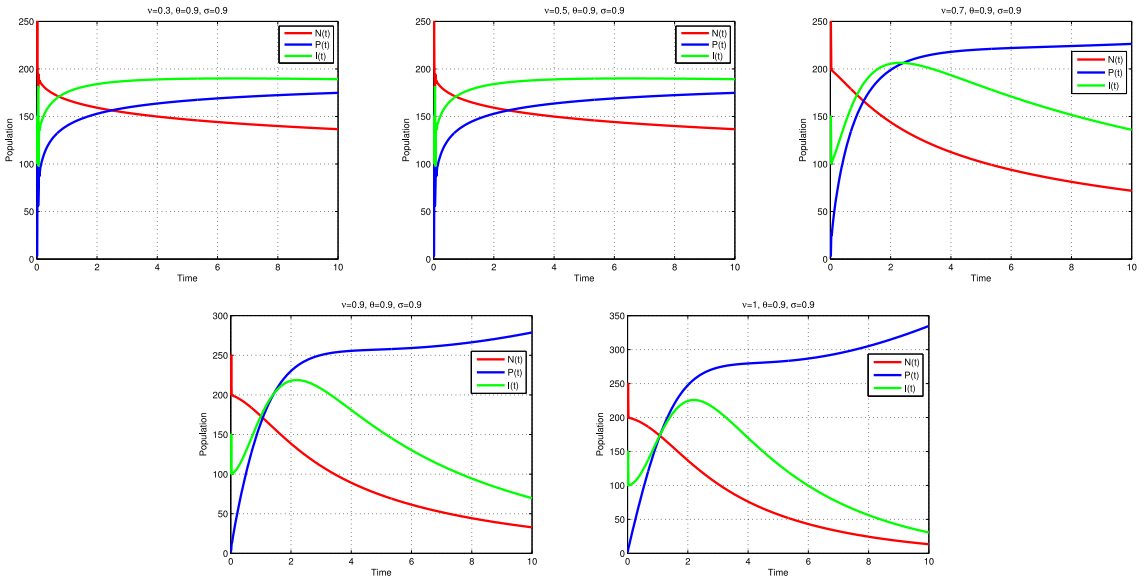

Fig. 13. Plots of state variables $N(t), P(t)$, and $I(t)$ for $\varrho = \sigma = 0.9$ and different values of γ.

CRediT authorship contribution statement

Chinedu Izuchukwu: Writing – review & editing, Writing – original draft, Visualization, Methodology, Formal analysis, Conceptualization. **David Amilo:** Writing – review & editing, Validation, Software, Resources. **Khadijeh Sadri:** Writing – review & editing, Validation, Software, Resources. **Hao-Ren Yao:** Writing – review & editing, Validation, Supervision, Investigation. **Jen-Chih Yao:** Writing – review & editing, Validation, Supervision, Resources, Project administration.

Declaration of competing interest

The authors declare that they have no known competing financial interests or personal relationships that could have appeared to influence the work reported in this paper.

Acknowledgments

Chinedu Izuchukwu is partially supported by the DSI-NRF Centre of Excellence in Mathematical and Statistical Sciences (CoE-MaSS), South Africa (Grant Number 2024-032-OPA) . Opinions expressed and conclusions arrived at are those of the author and are not necessarily to be attributed to the CoE-MaSS. Jen-Chih Yao was partially supported by the grant NOST-113-2115-M-039-001. The authors thank the reviewers for providing valuable comments and useful suggestions that helped improve the earlier version.

Appendix A. Calculating the convergence rate numerically and comparing results with those obtained from method (1.8)

We consider the following simple fractional-order differential equation:

$$ {}_0^c D_t^{\gamma} y(t) + y(t) = t^2 + \frac{2\, t^{2-\gamma}}{\Gamma(3-\gamma)}, \quad t \in [0,1],\ \gamma \in (0,1], \tag{A.1} $$

with the initial condition as $y(0) = 0$ and exact solution is $y(t) = t^2$. The maximum absolute errors (MAE) are calculated for different step sizes h, $\gamma = 0.5, 0.9$, $\sigma = 0.01$, and $\varrho = 0.1$ and are listed in Tables 2 and 3. The following relation computes the convergence rate (CR):

$$ CR_i = \left| \frac{\ln(e_{i+1}/e_i)}{\ln(h_{i+1}/h_i)} \right|, $$

where e_i is the absolute error corresponding to the step size h_i. As observed, the convergence rate approaches 1. Next, we compare the results obtained from the proposed method with those from the method described in (1.8). The MAEs are seen in Table 4 for $\sigma = 0.01, \gamma = 0.5$, and different values of step size h. As observed, the results obtained from the proposed scheme are more accurate than those produced by Method (1.8). In Table 2, the maximum absolute error is 3.0517×10^{-5} for $h = 2^{-15}$, whereas in Table 4, it is 0.0038. As the step size decreases, the error increases. The exact, approximate, and absolute error functions are shown in Fig. 14. The absolute error computed using the proposed method is smaller than that of Method (1.8).

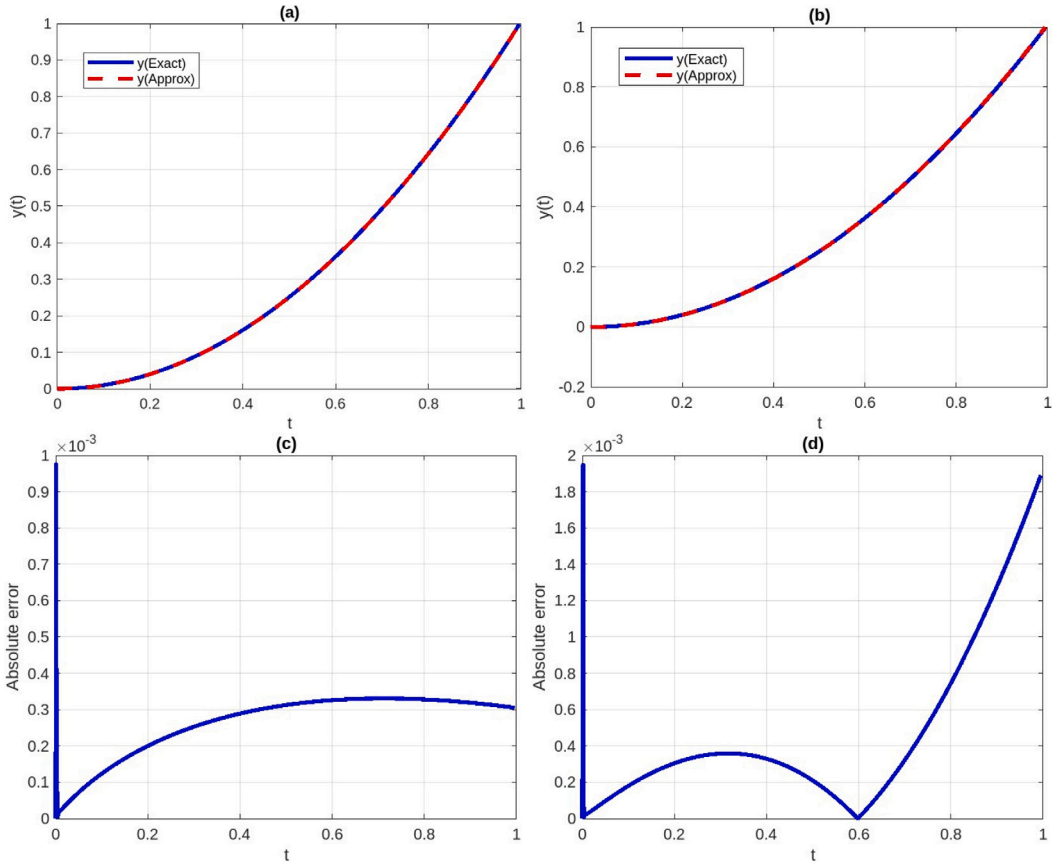

Fig. 14. Plots of (a) Exact and approximate solutions obtained from the proposed algorithm for $\sigma = 0.01, \varrho = 0.1, \gamma = 0.5, h = 2^{-10}$, (b) Exact and approximate solutions obtained from Method (1.8) $\sigma = 0.01, \gamma = 0.5, h = 2^{-10}$, (c) Absolute error function related to the proposed algorithm, (d) Absolute error function related to (1.8).

Table 2
Convergence rate of the proposed algorithm for $\gamma = 0.5$.

h	MAE	CR	h	MAE	CR
2^{-4}	5.9477×10^{-2}	–	2^{-5}	3.0273×10^{-2}	0.9743
2^{-6}	1.5381×10^{-2}	0.9769	2^{-7}	7.7515×10^{-3}	0.9886
2^{-8}	3.8910×10^{-3}	0.9943	2^{-9}	1.9493×10^{-3}	0.9972
2^{-10}	9.7509×10^{-4}	0.9993	2^{-11}	4.8804×10^{-4}	0.9985
2^{-12}	2.4408×10^{-4}	0.9996	2^{-13}	1.2206×10^{-4}	0.9998
2^{-14}	6.1031×10^{-5}	0.99998	2^{-15}	3.0517×10^{-5}	0.99993

Table 3
Convergence rate of the proposed algorithm for $\gamma = 0.9$.

h	MAE	CR	h	MAE	CR
2^{-4}	5.8594×10^{-2}	–	2^{-5}	3.0273×10^{-2}	0.9527
2^{-6}	1.5381×10^{-2}	0.9769	2^{-7}	7.7515×10^{-3}	0.9886
2^{-8}	3.8910×10^{-3}	0.9943	2^{-9}	1.9493×10^{-3}	0.9972
2^{-10}	9.7561×10^{-4}	0.9986	2^{-11}	4.8804×10^{-4}	0.9993
2^{-12}	2.4408×10^{-4}	0.9996	2^{-13}	1.2206×10^{-4}	0.9998
2^{-14}	6.1031×10^{-5}	0.99991	2^{-15}	3.0517×10^{-5}	0.99996

Table 4
Maximum absolute errors obtained from Method (1.8) for $\gamma = 0.5, \sigma = 0.01$ and different values of step size.

h	MAE	h	MAE	h	MAE
2^{-4}	0.1094	2^{-8}	0.0078	2^{-12}	0.0034
2^{-5}	0.0586	2^{-9}	0.0039	2^{-13}	0.0036
2^{-6}	0.0303	2^{-10}	0.0019	2^{-14}	0.0037
2^{-7}	0.0154	2^{-11}	0.0029	2^{-15}	0.0038

Table 5
Maximum absolute errors obtained for different choices of ϱ.

ϱ	MAE	ϱ	MAE	ϱ	MAE
0.09	0.4282	0.6	0.1635	0.93	0.0082
0.1	0.3776	0.7	0.1272	0.94	0.0053
0.2	0.3299	0.8	0.0928	0.95	0.0024
0.3	0.2848	0.9	0.0601	**0.97**	$\mathbf{9.7561 \times 10^{-4}}$
0.4	0.2421	0.91	0.0290	0.98	0.0148
0.5	0.2017	0.92	0.0141	0.99	0.0286

Appendix B. Effect of the inertia parameter on acceleration

Consider (A.1) again. We solve this problem with the proposed algorithm for $h = 2^{-10}, \gamma = 0.9$, and different values of the inertia parameter ϱ. The maximum absolute errors (MAEs) are seen in Table 5. It seems the best choice for this problem is $\varrho = 0.97$. Approaching values of ϱ to 0.97 leads to smaller absolute errors.

Data availability

No data was used for the research described in the article.

References

[1] Hoai PT. A new proximal gradient method for solving mixed variational inequality problems with a novel explicit stepsize and applications. Math Comput Simulation 2025;229:594–610.
[2] Jolaoso LO, Shehu Y, Yao JC. Inertial extragradient type method for mixed variational inequalities without monotonicity. Math Comput Simulation 2022;192:353–69.
[3] Li C, Lei S, Ding L, Xu Y, Wu X, Wang H, , Li L. Global burden and trends of lung cancer incidence and mortality. Chin Med J 2023;136(13):1583–90.
[4] Kothari K, Mehta U, Prasad R. Fractional-order system modeling and its applications. J Eng Sci Technol Rev 2019;12(6).
[5] Petráš I. Fractional-order nonlinear systems: modeling, analysis and simulation. Springer Science & Business Media; 2011.
[6] Debbouche N, Ouannas A, Momani S, Cafagna D, Pham VT. Fractional-order biological system: chaos, multistability and coexisting attractors. Eur Phys J: Spec Top 2021;1–10.
[7] Ndenda JP, Njagarah JBH, Shaw S. Role of immunotherapy in tumor-immune interaction: Perspectives from fractional-order modelling and sensitivity analysis. Chaos Solitons Fractals 2021;148:111036.
[8] Lions PL, Mercier B. Splitting algorithms for the sum of two nonlinear operators. SIAM J Numer Anal 1979;16:964–79.
[9] Passty GB. Ergodic convergence to a zero of the sum of monotone operators in Hilbert spaces. J Math Anal Appl 1979;72:383–90.
[10] Tseng P. A modified forward–backward splitting method for maximal monotone mappings. SIAM J Control Optim 2000;38:431–46.
[11] Briceño-Arias LM, Combettes PL. A monotone skew splitting model for composite monotone inclusions in duality. SIAM J Optim 2011;21:1230–50.
[12] Vũ BC. A variable metric extension of the forward–backward–forward algorithm for monotone operators. Numer Funct Anal Optim 2013;34:1050–65.
[13] Vũ BC. Almost sure convergence of the forward–backward-forward splitting algorithm. Optim Lett 2016;10:781–803.
[14] Lions JL. Optimal control of systems governed by partial differential equations. Berlin: Springer; 1971.
[15] Malitsky Y, Tam MK. A forward–backward splitting method for monotone inclusions without cocoercivity. SIAM J Optim 2020;30:1451–72.
[16] Izuchukwu C, Reich S, Shehu Y. Convergence of two simple methods for solving monotone inclusion problems in reflexive Banach spaces. Results Math 2022;77. http://dx.doi.org/10.1007/s00025-022-01694-5.
[17] Cevher V, Vũ BC. A reflected forward–backward splitting method for monotone inclusions involving Lipschitzian operators. Set-Valued Var Anal 2021;29:163–74.
[18] Malitsky YV. Projected reflected gradient methods for monotone variational inequalities. SIAM J Optim 2015;25:502–20.
[19] Malitsky Y. Proximal extrapolated gradient methods for variational inequalities. Optim Methods Softw 2018;33:140–64.
[20] Izuchukwu C, Reich S, Shehu Y. Relaxed inertial methods for solving the split monotone variational inclusion problem beyond co-coerciveness. Optimization 2023;72:607–46.
[21] Nesterov Y. A method of solving a convex programming problem with convergence rate $O(1/k^2)$. Sov Math Dokl 1983;27:372–6.
[22] Polyak BT. Some methods of speeding up the convergence of iterates methods. U. S S R Comput Math Phys 1964;4(5):1–17.
[23] Tran-Dinh Q, Zhu Y. Non-stationary first-order primal–dual algorithms with faster convergence rates. SIAM J Optim 2020;30. http://dx.doi.org/10.1137/19M1293855.
[24] Lorenz DA, Pock T. An inertial forward–backward algorithm for monotone inclusions. J Math Imaging Vision 2015;51:311–25.
[25] Moudafi A, Oliny M. Convergence of a splitting inertial proximal method for monotone operators. J Comput Appl Math 2003;155:447–54.
[26] Su W, Boyd S, Candes EJ. A differential equation for modeling Nesterov's accelerated gradient method: theory and insights. J Mach Learn Res 2016;17:1–43.
[27] Goodfellow I, Bengio Y, Courville A. Deep learning. MIT Press; 2016.
[28] Opial Z. Weak convergence of the sequence of successive approximations for nonexpansive mappings. Bull Am Math Soc 1967;73:591–7.

[29] Kothari K, Mehta UV, Prasad R. Fractional-order system modeling and its applications. J Eng Sci Technol Rev 2019;12(6):1–10.
[30] Dulf EH, Vodnar DC, Danku A, Muresan CI, Crisan O. Fractional-order models for biochemical processes. Fractal Fract 2020;4(2):12.
[31] Caponetto R. Fractional order systems: modeling and control applications. Vol. 72, World Scientific; 2010.
[32] Amilo D, Sadri K, Kaymakamzade B, Hincal E. A mathematical model with fractional-order dynamics for the combined treatment of metastatic colorectal cancer. Commun Nonlinear Sci Numer Simul 2024;130:107756.